

The Probe of Inflation and Cosmic Origins

A Space Mission Study Report
December, 2018

Principal Investigator:

Steering Committee:

Executive Committee:

Contributors:

Endorsers:

1 Executive Summary (2 pg, Hanany)

48 remaining pages are distributed 29/19: 29 pages for science (including foregrounds and systematics), 19 for instrument, technology, mission, management and cost.

2 Science

2.1 Introduction (1.5 pgs)

Recent theoretical developments and measurements of the cosmic microwave background (CMB) have uncovered tremendous potential for new discoveries over the next 10-20 years. The new discoveries are promising to be no less revolutionary than those attained to date. Many of the potential new discoveries are based on deeper measurements of the spatial pattern of the CMB's polarization. **would like to make this broader to not shortchange T-science, but still connect to E, B in the next paragraph.**

The angular power spectra of sky-based Q and U polarization Stokes parameters are commonly recast in terms of curl-free E mode and gradient-free B mode patterns. E modes are generated by either scalar, such as density, perturbations in the early Universe or by tensor, such as gravitational wave, perturbations. B modes are only generated through tensor perturbations. The Probe of Inflation and Cosmic Origins (PICO) is an imaging polarimeter designed to survey the entire sky at frequencies between 21 and 800 GHz with 57 times the polarization sensitivity of the *Planck* mission, a sensitivity surpassing any other current or planned CMB instrument.

Fluctuations of the space-time metric during the epoch of inflation, near the Planck time, have generated gravitational waves that embed a unique B-mode signature on the polarization of the CMB. A detection of the signal "would be a watershed discovery", a quote from the 2010 decadal panel report [?], as it would be our first signal from the epoch of quantum gravity at the beginning of the Universe. The signal would also give strong clues about the nature of inflation, as the B-mode signal is proportional to the energy scale of inflation through a parameter commonly labeled r , the tensor-to-scalar ratio. The combination of data from *Planck* and the BICEP/Keck Array give the strongest constraint to date $r < 0.06$ (95%) [?]. This limit has already ruled out several models for the inflaton potential [?]. But the measurements have also revealed that emission within our own galaxy is a source of confusion that must be separated with high fidelity before definitive discovery, or stronger upper limits, can be claimed [?]. PICO has the frequency coverage and sensitivity to measure and separate sources of foreground confusion and is thus poised to detect or place unprecedented constraints on the physics of inflation. **SO2 in the STEM is about measuring ns and nrun. should we mention them here?**

suggest to insert words about star formation history here. This will introduce tau, which we need in the next paragraph A few hundred million years after the Big Bang, the neutral hydrogen gas permeating the Universe was reionized by photons emitted by the first luminous sources to have formed. The nature of these sources (e.g., star-forming galaxies or high-redshift quasars) and the exact history of this epoch are key missing links in our cosmological knowledge. Various measurements have indicated that reionization concluded by $z \approx 6$, but its onset at higher redshift is poorly constrained. PICO will yield a breakthrough in this context via a cosmic-variance-limited measurement of τ , the optical depth to reionization, which can only be directly measured in large-scale CMB polarization fluctuations. *Planck* found $\tau = 0.054 \pm 0.007$, but PICO will provide τ

with uncertainty $\sigma(\tau) = 0.002$, limited only by cosmic variance¹. The only proven method to date for measuring this signal, which requires exquisite control of systematics and foreground contamination, is the space-based CMB platform, as realized in PICO.

Lensing of the CMB photons by structures as they traverse the Universe provides a projected map of all the matter in the universe from the epoch of decoupling until today. The non-zero mass of neutrinos affects the clustering of matter and thus can be inferred from maps of the projected matter distribution. The quantity that can specifically be inferred is the sum of the neutrino masses. The current constraint from the combination of *Planck*(including CMB lensing) and large-scale structure data is $\sum m_\nu < 0.12$ eV (95% C.L.). This is approaching the minimum summed mass allowed in the inverted neutrino hierarchy (≈ 0.1 eV) and is within a factor of two of the minimal mass allowed in the normal hierarchy (≈ 0.06 eV). A detection thus appears imminent. However, the precision of determining the neutrino mass scale, using the CMB or *any* other cosmological probe, is limited by knowledge of τ , due to the strong degeneracy between τ and the amplitude of matter fluctuations. A direct measurement of τ via the large-scale E-mode polarization signal is thus required in order to break this degeneracy and enable a detection of the sum of the neutrino masses. The current uncertainty from *Planck*, $\sigma(\tau) \approx 0.007$, will already limit neutrino mass constraints from cosmological experiments in the next five years; in order to go beyond this, a cosmic-variance-limited measurement with $\sigma(\tau) = 0.002$ must be achieved. Due to its multi-frequency capabilities, all-sky coverage, and excellent control of systematics, PICO is the ideal experiment to achieve this goal.

The CMB also offers a unique window into the *thermal* history of the universe, from the time of reheating through today. It is during these eras that the matter and radiation that fill the universe were produced and evolved to form the structures observed at low redshifts. Measurements of the CMB on small angular scales are sensitive to the many components that make up the universe including the baryons, cosmic neutrinos, dark matter, and a wide variety of particles motived by extensions of the Standard Model.

The Standard Model of particle physics posits three neutrino families, but it also allows for additional light, relativistic particles, if they existed early enough during the evolution of the Universe. We count the total number light particles thermalized in the early universe using N_{eff} . Light particles thermalized in the early universe leave a universal contribution to N_{eff} that is sensitive to the freeze-out temperature and then spin of the particle. A mission like PICO holds the promise to reach back to times when the temperature of the universe was orders of magnitude hotter than we have probe today. Such a measurement would shed light on the history of the universe at those very early times and can address important questions about the particles and forces in the Standard Model and Beyond. The history of the universe prior to a few seconds is still largely unexplored observationally and an PICO could reveal important clues to the nature of the fundamental laws and our cosmic origins.

The current measurement of $N_{\text{eff}} = 2.99 \pm 0.17$ from *Planck* is sensitive to particles thermalized after the QCD phase transitions. Reaching much earlier time is possible with PICO because of much lower noise levels in polarization. Larger sky coverage further improves the statistics and compensates for the lower resolution compared to ground based measurements. These features are advantageous not only for N_{eff} for any new physics present in the primary CMB and/or lensing potential. Of particular interest is the nature of dark matter and its interactions, which can be

¹The cosmic variance limit is the statistical limit arising from observing a single Universe.

manifest itself in any or all of these probes, depending on the details physics of the dark sector.

the paragraph below covers a lot of ground, but the anticipated impact is not clear. do we want to mention cluster counts? the impact of source counts? Gianfranco thinks pico is unique, but this is not clear. Need to say what PICO will do for these topics - Nick, thoughts? NB: I gave this a shot Secondary anisotropies in the CMB provide a wealth of information on the growth and evolution of structure in our universe. CMB lensing, the thermal and kinematic Sunyaev-Zel'dovich (SZ) effects, and extragalactic point sources all contribute significantly to the CMB intensity fluctuations on small angular scales (note that lensing is also present in polarization fluctuations). The all-sky, projected mass map reconstructed from CMB lensing that PICO will provide can be correlated with tracers of large-scale structure to tomographically probe the growth of structure at unprecedented signal-to-noise. The thermal SZ effect provides a map of the integrated free electron pressure along the line of sight, and the peaks of this map trace the locations of all galaxy clusters in the universe. PICO will find all the massive, virialized, galaxy clusters at any redshift. The epoch of reionization imprints information in the statistical moments of the kinematic SZ signal. The combination of these statistical moments with its cosmic variance limited τ measurement, PICO will provide information on the nature of the sources responsible for reionization. Pico will provide a full sky catalog of tens of thousands of extragalactic millimeter and sub-millimeter point sources, which are beacons for active galactic nuclei (in the radio) and dust emission from vigorously star-forming galaxies at $z \sim 2$ and earlier (in the far-IR).

need to add words about galactic science

2.2 Science Objectives (17.5 pgs)

The Science Traceability Matrix can be found in Table 1.

2.2.1 Fundamental Physics (6 pgs, Flauger, Green)

Inflation and Gravitational waves

add citations to the text? Measurements of the CMB together with Einstein's theory of general relativity imply that the observed density perturbations must have been created long before the CMB was released, and rather remarkably even before the universe became filled with a hot and dense plasma of fundamental particles. The mechanism generating these perturbations, which evolved to fill the Universe with structures, is one of the most compelling open questions in cosmology.

While the dynamics of the plasma produces some amount of gravitational waves, the amplitude is predicted to be too small to be detected in existing or planned experiments. Therefore any imprint of gravitational waves on the CMB detected by PICO would constitute evidence for gravitational waves from the same primordial period that created the density perturbations. the connection with gravitational waves is not completely clear Because the dynamics of gravitational waves is essentially unaffected by the plasma physics, they would be a pristine relic left over from the earliest moments of our universe, and their properties would shed light on the mechanism that created the primordial perturbations. Knowledge of the strength of the signal and its statistical properties would transform our understanding of many areas of fundamental physics.

Inflation, a period of nearly exponential expansion of the early universe, is the leading paradigm explaining the origin of the primordial density perturbations. It predicts a nearly scale invariant spectrum of primordial gravitational waves originating from quantum fluctuations. Thus, a detection of these gravitational waves would be the first detection of phenomenon associated with quantum gravity. Because the spectrum is scale-invariant, one may hope to detect primordial

Table 1: Science Traceability Matrix

Science Goals from NASA Science Plan	Science Objectives	Scientific Measurement Requirements			Instrument (single instrument, single mode)		Mission Functional Requirements	
		Model Parameters	Physical Parameters	Observables	Functional Requirements	Projected Performance		
Explore how the universe began (Inflation)	SO1. Probe the physics of the big bang by detecting the energy scale at which inflation occurred if it is above 4×10^{15} GeV, or place an upper limit if it is below (§ 2.2.1, Figure TBD)	Tensor-to-scalar ratio r : $\sigma(r) < 5 \times 10^{-5}$ at $r = 0$; $r < 10^{-4}$ at 95% confidence level	CMB polarization B -mode power spectrum for modes $2 < l < 300$ to cosmic variance limit, and CMB lensing power spectrum for modes $2 < l < 1000$ to cosmic variance limit	Linear polarization across $60 < v < 300$ GHz over entire sky	Frequency coverage [for foreground separation]: v_c from 30 to 500 GHz. Frequency resolution: $\Delta v/v_c = 25\%$. Sensitivity: See Table ??.	Frequency coverage: See Table ??. Combined instrument weight of $< 0.7 \mu\text{K}_{\text{CMB}} \sqrt{s}$. Angular resolution [for delensing and foreground separation]: FWHM = $6.2' \times (155 \text{ GHz}/v_c)$. Sampling rate: $(3/\text{BeamFWHM}) \times (336'/\text{s})$. Polarization systematics?	Sun-Earth L2 orbit with Sun-Probe-Earth $< 15^\circ$. 5 yr survey with $\geq 95\%$ survey efficiency.	
	SO2. Probe the physics of the big bang by excluding classes of potentials as the driving force of inflation (§ 2.2.1, Figure TBD)	Spectral index (n_s) and its derivative (n_{run}): $\sigma(n_s) < 0.0015$; $\sigma(n_{\text{run}}) < 0.002$	CMB polarization B -mode power spectrum for modes $2 < l < 1000$ to cosmic variance limit					
Discover how the universe works (Neutrino Mass and Neff)	SO3. Determine the sum of neutrino masses (Σm_ν): $\Sigma m_\nu < 15$ meV with DESI or Euclid; $\Sigma m_\nu < X$ meV alone	Sum of neutrino masses (Σm_ν): $\Sigma m_\nu < 15$ meV with DESI or Euclid; $\Sigma m_\nu < X$ meV alone	CMB polarization B -mode power spectrum for modes $2 < l < 4000$ to cosmic variance limit; CMB intensity maps (to give Compton Y map from which we extract clusters)	Intensity and linear polarization across 60–400 GHz over entire sky	Frequency resolution: $\Delta v/v_c = 25\%$. Sensitivity: See Table ??. Combined instrument weight of $0.46 \mu\text{K}_{\text{CMB}} \sqrt{s}$. Angular resolution: See Table ??. FWHM = $6.2' \times (155 \text{ GHz}/v_c); 1.1'$ for $v_c = 799$ GHz. Sampling rate: See Table ??. ($3/\text{BeamFWHM}) \times (336'/\text{s})$	Full sky survey: Spin instrument 1 rpm; Boresight 69° off spin axis; Spin axis 26° off anti-Sun line, precessing $360^\circ / 10$ hr.		
	SO4. Tightly constrain the thermalized fundamental particle content of the early Universe (§ 2.2.1, Figure TBD)	Number of neutrino effective relativistic degrees of freedom (N_{eff}): $\sigma(N_{\text{eff}}) < 0.03$	CMB temperature and E -mode polarization power spectra $2 < l < 4000$ to cosmic variance limit	Intensity and linear polarization across 60–300 GHz over entire sky				
Explore how the universe evolved (reionization)	SO5. Distinguish between models that describe the formation of the earliest stars in the universe (§ 2.2.2, Figure TBD)	Optical depth to reionization (τ): $\sigma(\tau) < 0.002$	CMB polarization E -mode power spectrum for modes $2 < l < 20$ to cosmic variance limit; T power spectrum and Compton Y maps.	Intensity and linear polarization across 60–300 GHz over entire sky (role of intensity maps at high ℓ to be clarified)	Enveloped by SO1–4, and less driving: Angular resolution $< 1^\circ$ at XX GHz (role of intensity maps at high ℓ to be clarified). Combined instrument weight of $< 0.86 \mu\text{K}$ arcmin	Pointing control: Spin axis $60'$ (3σ , radial). Spin 1 ± 0.1 rpm (3σ) Pointing stability: Drift of spin axis $< 1'/1\text{min}$ (3σ , radial); Jitter $< 20''/20$ ms (3σ , radial).		
	SO6. Determine if magnetic fields are the dominant cause of low star formation efficiency in our Galaxy. (§ 2.2.3, Figure TBD)		The turbulence power spectrum on scales 0.05–100 pc (from cores to diffuse cloud envelopes). Magnetic field strength (B) as a function of spatial scale and density. Hydrogen column density. Gas velocity dispersion.	Intensity and linear polarization with < 1 pc resolution for thousands of molecular clouds and < 0.05 pc for the 10 nearest molecular clouds.			Pointing knowledge (telescope boresight): $10''$ (3σ , each axis) from spacecraft attitude $1''$ (3σ , each axis) final reconstructed Return and process instrument data: 1.5 Tbits/day (after 4x compression) Thermally isolate instrument from solar radiation and from spacecraft bus	
Explore how the universe evolved (Galactic structure and dynamics)	SO7. Constrain the temperatures and emissivities characterizing Milky Way's interstellar diffuse dust.	Intrinsic polarization fractions of the warm and cold components of the diffuse interstellar medium to accuracy better than 2% when averaged over 10 arcmin pixels. Temperatures and spectral indices of the two dust components to an accuracy better than ??%	Fractional polarization and intensity as a function of frequency	Intensity and linear polarization maps in 12 frequency bands between 108 and 800 GHz.	Enveloped by SO1–4, except: Angular resolution: $\leq 1.1'$ (at highest frequency) Sensitivity at 800 GHz: 27.4 kJy/sr Saturation/Dynamic range?			
	SO8. Determine the role of energy feedback in the evolution of Milky Way's interstellar medium.	Ratio of turbulent energy to magnetic energy (Alfvén Mach number Ma) on scales 0.03–100 pc $\sigma(\text{Ma}) < ??$	The turbulence power spectrum on scales 0.03–100 pc in the neutral ISM. Magnetic field strength (B) as a function of spatial scale and density. Neutral hydrogen velocity dispersion.	Maps of polarization with $1'$ resolution over the entire sky.				

gravitational waves over a wide range of frequencies including, for example, at LIGO or LISA frequencies. However, as a consequence of the expansion of the universe, the energy density in the gravitational waves rapidly dilutes with increasing frequency, and observations of the CMB provide the easiest, and for the foreseeable future only way to detect these gravitational waves.

The strength of the signal, often quantified by the tensor-to-scalar ratio r , is a direct measure of the expansion rate of the universe during inflation. Together with the Friedmann equation, this reveals one of the most important characteristics of inflation, its energy scale. PICO will be able to detect primordial gravitational waves if inflation occurred at an energy scale of at least 4×10^{15} GeV. also quote an r value so as to connect to the introduction and current limits A detection would have profound implications for fundamental physics because it would provide evidence for a new energy scale, and would allow us to probe physics at energies far beyond the reach of terrestrial colliders.

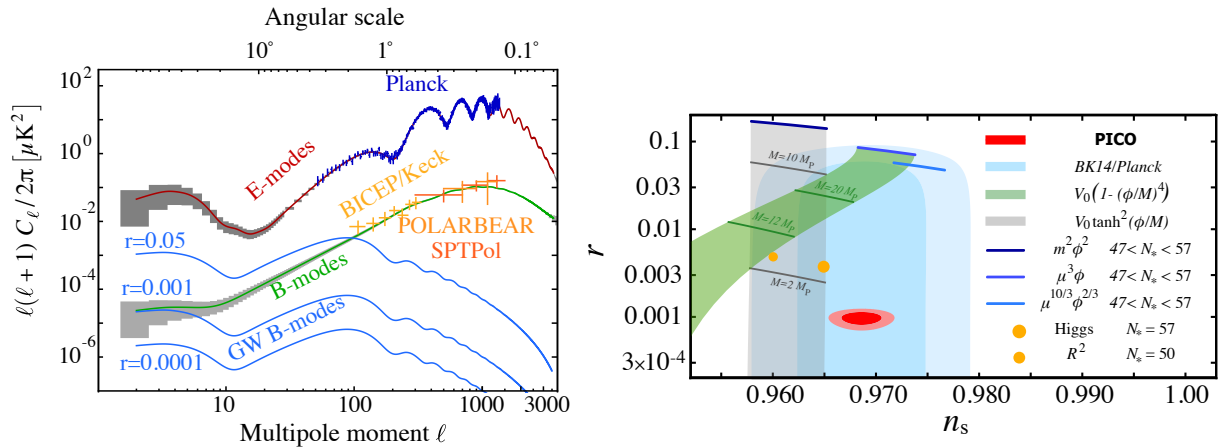


Figure 1: Predicted 1σ errors (grey) for determining the E (red) and B-mode (green) angular power spectra by PICO for an Inflationary gravity wave B-mode with $r = 0.001$. use $r=5e-4$? need to extend error bars to show high ℓ limit. Also shown are power spectra for other values (Solid blue), lensing B-mode detection from current experiments, and *Planck* measurements of the E mode. add noise, separate lensing + label, foregrounds?

The signal has two contributions, one on degree angular scales or multipoles of $\ell \sim 80$, typically referred to as the recombination peak, and another contribution for multipoles of $\ell \lesssim 20$ from the epoch of reionization; see the left panel of Figure 1. The contribution from reionization is expected to be strongest relative to the contributions from instrumental noise and ‘lensing’ (see Section ??). refer to where ever we talk about lensing. best illustrated with a figure. should we add the noise and lensing lines to Figure 1? No sub-orbital experiment has yet measured modes at $\ell < 40$. The temporal stability, absence of atmospheric noise, and full sky coverage offered by a satellite like PICO make it the most suitable instrument to reach these lowest multipoles.

There are two classes of slow-roll inflation that naturally explain the observed value of the spectral index of primordial fluctuations n_s . The first class is characterized by potentials of the form $V(\phi) \propto \phi^p$. This class includes many of the simplest models of inflation, some of which have already been strongly disfavored by existing observations; see the right panel of Figure 1. If the constraints on the spectral index tighten by about a factor 2 with the central value unchanged, and the upper limits on r improve by an order of magnitude, this class would be ruled out. complete

the argument about PICOs performance?

The second class is characterized by potentials that exponentially approach a plateau **not clear which plateau** and include R^2 inflation. This model predicts a tensor-to-scalar ratio of $r \sim 0.003$. All models in this class with a characteristic scale in the potential that is larger than the Planck scale predict a tensor-to-scalar ratio of $r \gtrsim 0.001$, **are there models in the class that have a characteristic scale smaller than the planck scale? what r do they predict?** and an experiment like CMB-S4 could exclude these scenarios. However, there are models such as the Goncharov-Linde model with a somewhat smaller characteristic scale that predict a tensor-to-scalar ratio of $r \sim 4 \times 10^{-4}$.

In the absence of a detection, PICO would limit the amount of gravitational waves to $r < 10^{-4}$ at 95% CL. This is stronger than current upper limits by three orders of magnitude, and stronger than those expected for the ground-based experiment CMB-S4 by an order of magnitude. **we need to mention the challenges of delensing, foregrounds, and systematics, and provide a link to these sections.**

Models of inflation, or the early universe more generally **need to phrase differently**, differ in their predictions for the scalar spectral index n_s and its scale dependence, often referred to as the running of the spectral index n_{run} . With its high resolution and low noise levels, PICO will improve the constraints on n_s and n_{run} by a factor of about two. In addition, PICO will probe the statistical properties of the primordial fluctuations over a wide range of scales with exquisite precision and improve constraints on departures from Gaussianity by a factor 2 – 3. **what about non-Gaussianity? Marcel is forecasting a level below 1**

Fundamental Particles: Light relics, Dark Matter, and Neutrinos

- **Light Relics** In the inflationary paradigm, the universe was reheated to temperatures of at least 10 MeV and perhaps as high as 10^{12} GeV. At these high temperatures, even very weakly interacting or very massive particles, such as those arising in extensions of the Standard Model of particle physics, can be produced in large abundances [1, 2]. As the universe expands and cools, the particles fall out of equilibrium, leaving observable signatures in the CMB power spectra. Through these effects the CMB is a sensitive probe of neutrino and of other particles' properties.

One particularly compelling target is the effective number of light relic particle species N_{eff} . The canonical value with three neutrino families is $N_{\text{eff}} = 3.046$. Additional light particles contribute a change to N_{eff} of $\Delta N_{\text{eff}} \geq 0.027 g$ where $g \geq 1$ is the number of degrees of freedom of the new particle [3, 4]. This correction to N_{eff} is a universal function of the decoupling temperature, with the range $0.07 g \geq \Delta N_{\text{eff}} \geq 0.027 g$ corresponding to decoupling from lower temperatures shortly after the QCD phase transition ($0.07g$) to higher temperatures near reheating ($0.027g$). A measurement of $\sigma(N_{\text{eff}}) \sim 0.03$ would at least two orders of magnitude higher decoupling temperatures for particles with spin for which $g \geq 7/4$ and will dramatically extend our knowledge of extensions of the Standard Model.

Performance forecasts for N_{eff} are shown in Figure 2. The two most important parameters for improving constraints are the fraction of sky observed f_{sky} and the noise. Achieving both larger f_{sky} and lower noise are strengths of PICO compared to other platforms. Our baseline mission would constraint $\Delta N_{\text{eff}} < 0.06$ at 95%. This large improvement over Planck ($\Delta N_{\text{eff}} < 0.28$ at 95%) would correspond a factor of 200 improvement in the limit on the decoupling temperature for any particle with spin. Constraints on N_{eff} in PICO are largely driven by the TE and EE spectra which are expected to be measured over large fractions of the sky. This target is achievable with PICO because the the larger sky fraction available from space compensates for the lower resolution required.

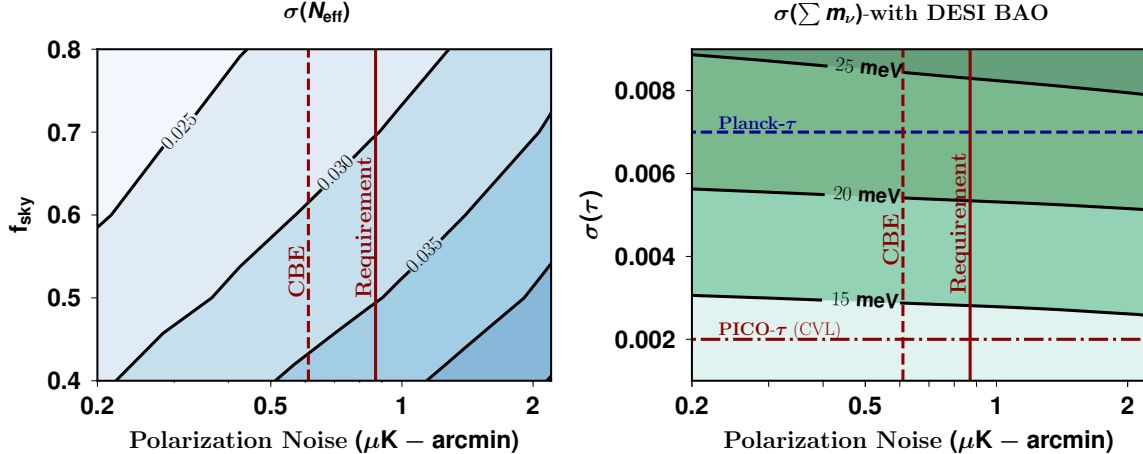


Figure 2: N_{eff} uncertainty as a function of noise and sky fraction (left) and sum of neutrino masses uncertainty as a function of noise and the uncertainty in the measurement of τ , for 0.7 sky fraction (right). The resolution assumed is $5'$. Vertical lines denote the expected performance of the baseline mission. The upper blue dashed line is the current *Planck* limit; the lower grey dashed line is the limit from cosmic variance limited measurement of τ . All forecasts assume internal delensing of the T and E -maps [5], including residual non-Gaussian covariances. The $\sum m_\nu$ forecasts include DESI BAO.

Many light relics of the early universe are not stable. They decay, leaving faint evidence of their past existence on other tracers. The relics with sufficiently long lifetime to survive few minutes, past the epoch of light element synthesis, leave a signature on the helium fraction Y_p . If they decay by the time of recombination, their existence through this period is best measured through the ratio of N_{eff} to Y_p . At both CBE and Requirement sensitivity, this measurement of Y_p improves on the current measurement of Y_p from astrophysical measurements of the primordial helium abundance and will offer a more sensitive window into the physics of BBN or any subsequent deviations from the Standard cosmology.

• **Dark Matter** Cosmological measurements have already confirmed the existence of one relic that lies beyond the Standard Model: dark matter. For a conventional WIMP candidate, the CMB places very stringent constraints on its properties through the signature of its annihilation on the T and E spectra [? ? ?]. Unfortunately, the limits on dark matter annihilation will be saturated by near term measurements [? ?].

Traditional nuclear-recoil based direct detection experiments search for dark matter (DM) in the form of weakly interacting massive particles, which are expected to experience rare interactions with heavily shielded target material placed deep underground [? ?]. The shielding of Earth's atmosphere and crust, however, places a “ceiling” on the sensitivity of direct detection searches to large scattering cross sections. Moreover, these experiments are only sensitive to DM masses above $\sim\text{GeV}$; new strategies are being considered to expand the reach to lower masses by using lighter target nuclei. An entirely complementary way to probe DM is to search for evidence of its interactions in cosmological data. Since a lower DM particle mass translates to a higher number density of scattering centers, CMB is particularly sensitive to the low-mass regime. In addition, the CMB does not experience a detection “ceiling” and is sensitive to large, nuclear-scale cross sections. Finally, the CMB directly probes physics of *cosmological* DM throughout cosmic history and does not rely on assumptions about the local DM density or phase-space distribution within the Milky Way.

Interactions between DM and protons in the early universe creates a drag force between the two cosmological fluids, damping acoustic oscillations and suppressing power in density perturbations on small scales. As a result, the CMB temperature, polarization, and lensing power spectra are suppressed at high multipoles, with respect to those in Λ CDM universe (see left panel of Figure 3 for illustration). This effect has been used to search for evidence of DM-proton scattering for heavy DM, using CMB and Lyman- α forest measurements [6? ?].

Recently, [?] presented the first cosmological search for DM particles with any mass down to a keV (orders of magnitude below the mass limits of direct detection experiments), and was followed by a number of similar studies [? ?]. In particular, [?] used *Planck* data to derive the first CMB limit on the non-relativistic effective theory of DM-proton scattering—a theoretical framework widely used in low-energy experiments to characterize all available phenomenologies for scattering through a heavy mediator. Similarly, [? ? ?] parametrized the interaction cross section through its power-law dependence on the relative particle velocity, and reported improved limits on a wide range of models. Furthermore, [?] developed an improved treatment of non-linear effects that arise in calculation of post-recombination scattering signals. This and related studies have enabled robust investigation of a scenario in which only a fraction of DM interacts—and tightly couples—with baryons (while the remaining fraction behaves as the standard cold DM fluid), leading to the first robust cosmological limits on an interacting DM sub-component [? ?]. Analyses of CMB data have also provided essential consistency tests of recent claims that the anomalous 21-cm signal reported by the EDGES collaboration [?] could be explained with late-time DM-baryon scattering [?]; see, for example, [? ?].

In Figure 3, we present current and projected upper limits on the DM-proton interaction cross section as a function of DM mass, for a spin-independent velocity-independent scattering (chosen as our fiducial model). Regions above the curves are excluded at the 95% confidence level. We compare current limits obtained from *Planck* (from ??) with projections for PICO sensitivity. We note that PICO can deliver a substantial improvement over the current limits, across the entire DM mass range considered.

Most of the constraining power in case of PICO (and ground-based next-generation measurements with similar white-noise levels) comes from the CMB lensing anisotropy measurement, while the temperature and polarization anisotropies contribute roughly equally to the projected constraint ???. Furthermore, ?? has also shown that DM-baryon scattering is easily distinguishable from most other new-physics effects sought by the CMB experiments (the neutrino mass, new light degrees of freedom, and DM annihilations) once the lensing anisotropy is measured at the level of PICO. PICO thus holds promise as a DM discovery tool.

• Neutrino Mass The origin and structure of the neutrino masses is one of the great outstanding questions about the nature of the Standard Model particles. Measurements of neutrinos in the lab have revealed much about the mass differences and mixing angles. Cosmology offers a measurement of the sum of the neutrino masses $\sum m_\nu$ through the gravitational influence of the non-relativistic cosmic neutrinos. The measurement of $N_{\text{eff}} = 2.99 \pm 0.17$ already confirms the existence of these neutrinos at $> 10\sigma$ but their mass implies that they contribute to the matter density at low redshifts. The best current constraint arises from a combination of Planck and BOSS barion acoustic oscillations (BAO) giving $\sum m_\nu < 0.12$ eV (95%) [citation](#).

Cosmological measurements are primarily sensitive to the suppression of power on small scales after the neutrinos become non-relativistic, which can be measured via CMB lensing or weak lensing in a galaxy survey. However, these measurements are limited by our knowledge of the

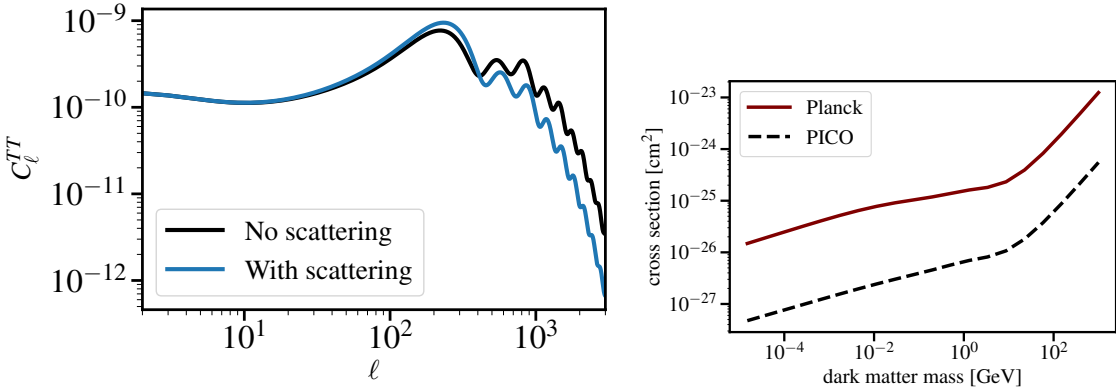


Figure 3: *Left:* Illustration of the effect of a velocity-independent spin-independent contact interaction between dark matter and baryons (with a cross section 100 times higher than the current upper limit from *Planck*) on the CMB temperature power spectrum (blue), compared to the CDM case (black). *Right:* Upper limits on DM-proton interaction cross section as a function of DM mass, for a spin-independent velocity-independent scattering. Areas above the curves are excluded at 95% confidence-level. Shown are the current limits from *Planck*(??) and a forecast for PICO.

amplitude of the primordial fluctuation power spectrum, A_s . In practice, CMB observations most directly constrain $A_s e^{-2\tau}$ and thus do not provide a high precision measurement of A_s or τ .

Although many surveys hope to detect $\sum m_\nu$, any detection of the minimum value expected from particle physics $\sum m_\nu = 58$ meV at more than 2σ will require a better measurement of τ . The best constraints on τ come from E modes with $\ell < 20$ which require measurements over the largest angular scales. To date, the only proven method for such a measurement is from space. The current limit of $\sigma(\tau) = 0.007$ is from *Planck* [10]. Forecasts for a CMB measurement of $\sum m_\nu$ using the lensing B mode [11] are shown in Figure 2. With the current uncertainty in τ one is limited to $\sigma(\sum m_\nu) \gtrsim 25$ meV; no other survey or cosmological probe would improve this constraint. But PICO will reach the cosmic variance limit of $\tau \sim 0.002$ and will therefore reach $\sigma(\sum m_\nu) < 15$ meV when combined with DESI's measurements of baryon acoustic oscillations [12]. Robustly detecting neutrino mass at $> 3\sigma$ in any cosmological setting is only possible with an improved measurement of τ like the one achievable with PICO. The measurement would give $\sum m_\nu > 0$ at greater than 4σ or would exclude the inverted hierarchy ($\sum m_\nu > 100$ meV) at 95% confidence, depending on the central value of the measurement. Lab-based measurement could determine the hierarchy before PICO but only cosmology can measure $\sum m_\nu$.

Fundamental Fields: Primordial Magnetic Fields and Cosmic Birefringence

- Primordial Magnetic Fields** One of the long standing puzzles in astrophysics is the origin of 1-10 μ G strength galactic magnetic fields [13]. Producing such fields through a dynamo mechanism would require a primordial seed field [14]. Moreover, μ G strength fields have been observed in proto-galaxies that are too young to have gone through the number of revolutions necessary for the dynamo to work. A primordial magnetic field (PMF), present at the time of galaxy formation, could provide the seed or even eliminate the need for the dynamo altogether. Specifically, a ~ 0.1 nG field in the intergalactic plasma would be adiabatically compressed in the collapse to form a ~ 1 μ G galactic field [15]. PMFs could have been generated in the aftermath of phase transitions in the early universe [16], during inflation [17, 18], or at the end of inflation [19]. A detection of

PMF would be a major discovery, signalling physics beyond standard models of particle physics and cosmology, and constraints on PMF offer a valuable tool for discriminating among different theories of the early universe [20, 21, 22]. While the PMF would be sustained by the primordial plasma well beyond recombination, with signatures at low redshifts, only seeing them in CMB would conclusively prove their primordial, as opposed to an astrophysical, origin.

The signature of PMF is detectable through Faraday rotation [23], which converts E modes into B modes, and through generating signatures in the BB power spectrum at high ℓ [24]. The current CMB bounds on PMF strength are $B_{1\text{Mpc}} < 1.2 \text{ nG}$ at 95% CL for the scale-invariant PMF spectrum [25]. PICO’s sensitivity and resolution would allow to probe PMFs as weak as 0.1 nG (1σ), a limit that already includes the effects of imperfect lensing subtraction, galactic foregrounds [26, 27, 28], and other systematic effects. It would, nevertheless, be an important improvement that will conclusively rule out the purely primordial (no dynamo) origin of the largest galactic magnetic fields.

- **Cosmic Birefringence** The simplest model for late-time acceleration of the universe is with a slowly-evolving scalar field – the quintessence [29]. Such a field generically couples to electromagnetism through a Chern Simons-like term, and causes linear polarization of photons propagating cosmological distances to rotate. This is known as cosmic birefringence [29]. The birefringence converts primordial E mode into B mode. It thus produces parity-violating TB and EB cross-correlations whose magnitude depends on the statistical properties of the rotation field in the sky [30, 31]. There are no theoretical predictions for the level of birefringence, but if observed, it would be evidence for physics beyond the standard model and a potential probe of dark-energy microphysics [31, 32, 33]. Using the sensitivity of only the 155 GHz, PICO will improve current constraints on cosmic birefringence (from POLARBEAR [34]) by a factor of 300. The constraints will be even stronger when including all frequency bands.

2.2.2 Cosmic Structure Formation and Evolution (4 pgs. Hill, Battaglia (& Alvarez))

The Formation of the First Luminous Sources

The reionization of the Universe, which according to current measurements takes place near a cosmic age of ~ 700 million years [?], imprints multiple signals in the temperature and polarization of the CMB. In polarization, the most important signal is an enhancement of power in the E -mode spectrum at large angular scales $\ell \lesssim 20$. This signal gives a direct measurement of the optical depth to the reionization epoch τ , and thus to the mean redshift of reionization Z_{re} , with very little degeneracy with other cosmological parameters; see Figure 4. The mean redshift of reionization Z_{re} (when 50% of the cosmic volume was reionized) depends sensitively on the nature of the ionizing sources. For example, it is currently unknown whether star-forming galaxies or more exotic sources such as supermassive black holes drove the reionization process. **is this THE question, or are there other examples? Would the answer change Z_{re} ?** Furthermore, the detailed shape of the low- ℓ E -mode power spectrum is sensitive to the reionization history itself (i.e., $d\tau/dz$), and will provide information beyond that captured in τ alone. For example, it has been argued that *Planck* data show evidence for an extended tail of reionization out to $z \approx 15\text{-}20$ [?]. A cosmic-variance-limited measurement of the large-scale E modes, as obtained by PICO, will settle this question.

Large-scale EE power spectrum measurements are a unique and crucial observable for many aspects of cosmology **which many**. If measurements of τ are not improved beyond the current uncertainties from *Planck*, inference of several new signals of cosmological physics (e.g., neutrino mass) will be severely hindered **which other new signals**. PICO is the ideal experiment to make this

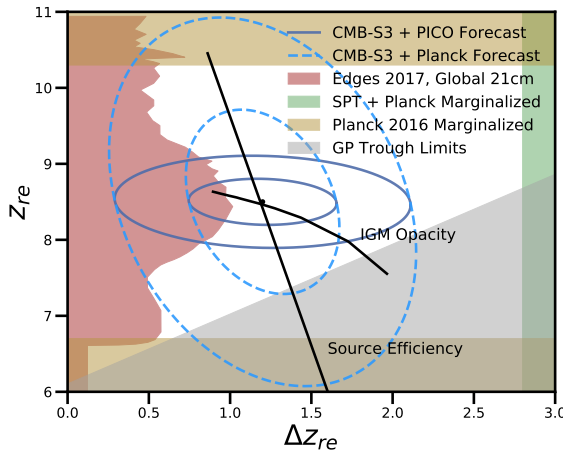


Figure 4: Summary of constraints on the mean redshift and duration of reionization. The forecasts show 68% and 95% confidence-level contours for PICO combined with CMB-S3 experiments and Planck combined with CMB-S3 experiments (dark blue and dashed blue, respectively). The solid black lines illustrate how the IGM opacity and source efficiency model parameters map onto this parameter space. The forecasted PICO constraints are compared to: current exclusion limits for the mean redshift of reionization from Planck, shown by the yellow bands ? ; recent exclusion limits from the global 21 cm signal measured by EDGES, shown with the red band ? ; exclusion limits from measurements of the Gunn-Peterson trough from fully absorbed Lyman α in quasar spectra, shown by the grey band ? ; exclusion limit on the duration of reionization from Planck and SPT data, shown by the green band ? .

measurement. Its noise level and frequency coverage permit a cosmic-variance-limited constraint on τ , i.e., $\sigma(\tau) \approx 0.002$, which we have verified with explicit forecasts including foregrounds.

In temperature, the most important imprint of reionization is that sourced at small angular scales by the “patchy” kinematic Sunyaev-Zel’dovich (kSZ) effect, due to the peculiar velocities of free electron bubbles around ionizing sources (e.g., galaxies or quasars). The total kSZ power spectrum receives contributions from both the patchy reionization signal and “late-time” sources, e.g., the intergalactic and intracluster media. The reionization and late-time signals are expected to have comparable amplitudes [? ? ?]. With constraints on the late-time contribution from other information (e.g., cross-correlations), effective small-scale foreground removal, and with the primary CMB TT power spectrum constrained by inference from the EE power spectrum [?]. The most directly constrained quantity is the duration of reionization, Δz_{re} . **if pico is not providing kSZ constraints, only S3 does, there is no need to dwell on it at all, I think. Nick, can you condense this?**

Fig. 4 presents forecasts for reionization constraints in the z_{re} - Δz_{re} parameter space obtained from PICO’s measurement of τ in combination with ground-based Stage-III (CMB-S3) constraints on the kSZ power spectrum. Constraints from existing Planck data and observations at other wavelengths are also presented. The PICO measurement of τ is essential for breaking degeneracies **does not appear to be borne out by the figure** and allowing simultaneous, precise constraints to be placed on both the mean redshift and duration of reionization. Fig. 4 also shows curves of constant source efficiency (i.e., the efficiency of ionizing photon production) and constant intergalactic medium opacity (i.e., the photon mean free path). PICO will allow simultaneous constraints to be placed on these physical parameters, yielding important information on the nature of the first luminous sources (e.g., star-forming galaxies or quasars predict significantly different values for these parameters).

In addition to these signals, reionization also leaves specific non-Gaussian signatures in the CMB. In particular, patchy reionization induces non-trivial 4-point functions in both temperature [?] and polarization [?]. The temperature 4-point function can be used to separate reionization and late-time kSZ contributions. Combinations of temperature and polarization data can

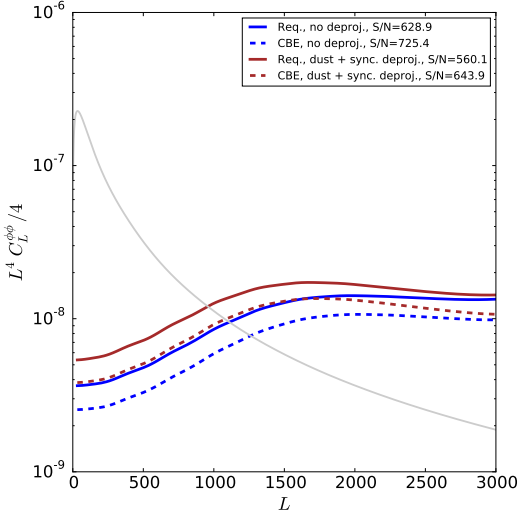


Figure 5: if we are using this figure: make the grey black, cut top scale at $3e-7$; increase size of fonts and legend; use 2 or 3 significant figures (not 4) The theoretically predicted lensing power spectrum $C_L^{\phi\phi}$ (grey) and forecasted PICO noise levels, with (red), and without (blue) removal of foregrounds. PICO will make a map of ϕ at angular scales where the noise is below the signal.

be used to build quadratic estimators for reconstruction of the patchy τ field, analogous to CMB lensing reconstruction. These estimators generally require high angular resolution, but also rely on foreground-cleaned CMB maps. Thus, while PICO alone may not enable high S/N reconstructions, its high-frequency channels — which have better than 2 arcmin resolution and observe at frequencies that have yet to be demonstrated from the ground — will enable these estimators to be robustly applied to ground-based CMB data sets, a strong example of ground-space complementarity. if pico is complementarity by *only* providing foreground maps at sufficiently high resolution, I think we should move this to the ‘complementarity’. It is not a direct science goal or outcome.

The Sections below need to be rearranged to match other Science Objective(s) from the STM, but to also relay the breadth of science reachable by PICO, even if those goals are not in the STM.

Structure Formation via Gravitational Lensing

Matter between us and the last-scattering surface deflects the path of photons through gravitational lensing, imprinting the 3-dimensional matter distribution across the volume of the universe onto the CMB maps. The specific quantity being mapped by the data is the projected gravitational potential ϕ that is lensing the photons. The lensing map is most sensitive to structures at redshift $z \simeq 2$. Using a map of ϕ , called the ‘lensing potential map’, we form the angular power spectrum $C_L^{\phi\phi}$, which depends on cosmological parameters why do we say that it depends on cosmological parameters? is that meant to connect to something later?. Both the temperature and polarization maps of the CMB, and by extension the angular power spectra, are affected by lensing.

Planck’s ϕ map had Signal to noise ratio (SNR) of ~ 1 per L mode, up to $L \simeq ?$. PICO’s map would represent true mapping, with SNR $\gg 1$ per each mode down to scales of approximately ten arcminutes; see Figure 5. On smaller scales, the map will still contain statistical information. While *Planck* had a signal-to-noise ratio (SNR) of 40 in the $C_L^{\phi\phi}$ power spectrum [35], the PICO combination of resolution, sensitivity and sky coverage enables a measurement with SNR of 638 and 737 for the required and CBE configurations, respectively. When accounting for possible foreground contamination, its broad frequency coverage leads to a reduction of SNR of less than 20%; see Figure 5.

Next two paragraphs section drafted by AVE with MS away - needs verification. The value of the reconstructed lensing map is immense, as has already been demonstrated with much lower SNR map from *Planck*. The unprecedented constraints on neutrino mass, discussed in Section ??

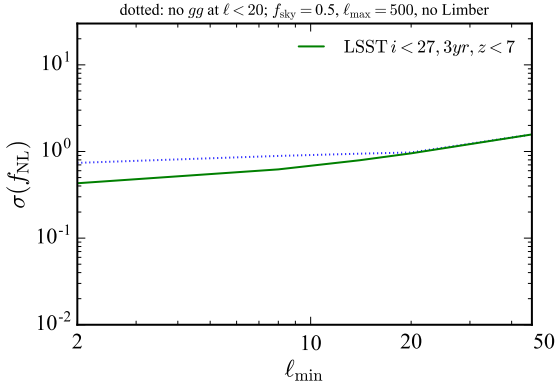


Figure 6: Forecasted sensitivity to the parameter describing primordial non-Gaussianity of the local type for the PICO CMB lensing map together with three years of the LSST survey, as a function of the minimal multipole used in the analysis. A value of $\sigma(f_{\text{NL}}) \simeq 1$ is a well-motivated theoretical target.

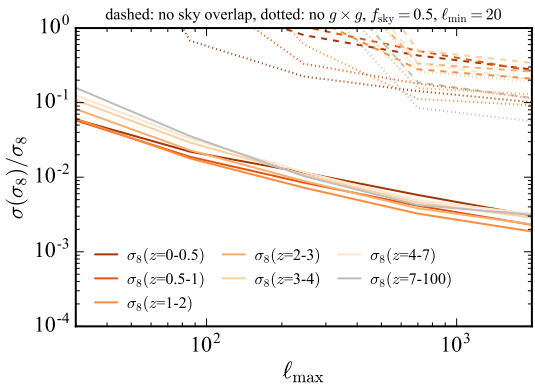


Figure 7: Forecasted sensitivity to the parameter describing the amplitude of structure in various redshift bins, as a function of the maximal multipole used in the analysis. Percent-level constraints on these parameters allow for stringent tests of physics beyond ΛCDM that modify the rate of growth of structure.

are a direct result of this deep map. Tomographic cross-correlations of the lensing map with samples of galaxies and quasars will yield constraints on structure formation. The measurements will constrain the properties of quasars and other high-redshift astrophysics, e.g., a precise determination of the quasar bias (and hence host halo mass) as a function of their properties, such as (non-)obscuration. The map will be cross-correlated with other large scale tracers to probe fundamental physics. For instance, one can use correlations between large scale structure tracers with different clustering bias factors to effectively cancel cosmic variance [42, 43] and constrain physics that affects the biasing of objects on large scales, such as primordial local non-Gaussianity [?]. In Fig. 6 we show the expected constraints for the CMB lensing field as reconstructed with PICO, in cross correlation with three years of the LSST survey. It can be seen that depending on the minimal multipole that can be used in the cross correlation, which is uncertain in both LSST and the PICO lensing map, the well-motivated theory target of $\sigma(f_{\text{NL}}) \simeq 1$ [44] can be within reach. **need to say why reaching this level is interesting.**

Using the same cross-correlation techniques, it is also possible to constrain the evolution of the amplitude of structure as a function of redshift. Figure 7 shows constraints on the amplitude of linear structures in several redshift bins. These measurements will yield constraints on dark energy, modified gravity, and neutrino mass. **do we have any quantitative constraints?** Note that this neutrino mass constraint is complementary to that inferred from the CMB lensing auto-power spectrum described earlier.

Lensing will also be used to weigh dark matter halos hosting galaxies, groups and clusters of galaxies **why do we want to weigh DM? let's motivate more broadly**. In this approach, known as halo lensing, we focus on the small scale effects of gravitational lensing around these objects [38,

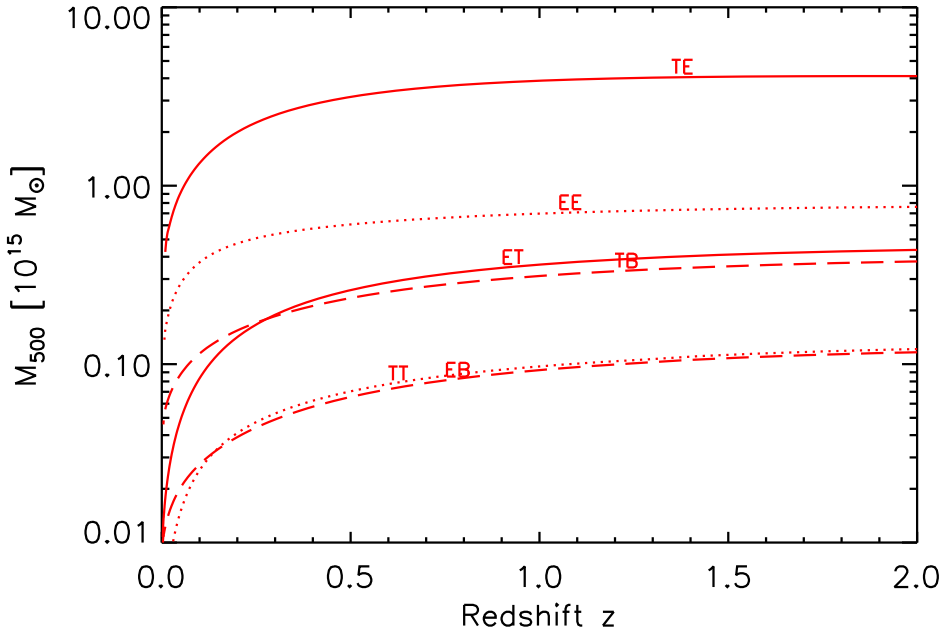


Figure 8: PICO sensitivity for CMB halo lensing. The different curves give the one-sigma sensitivity of an optimal mass filter [41] using different possible lensing estimators constructed from both temperature and polarization anisotropy measurements. The curves are flat at high redshift, demonstrating the essential property that CMB halo lensing can be applied over a very wide redshift range (well beyond the $z = 2$ limit of the figure). For PICO, the EB and TT estimators are roughly equivalent, offering important cross-validation of measurements because the systematics are very different for temperature and polarization.

39, 40]. The technique holds great potential for measuring halo masses out to high redshifts where gravitational lensing of galaxies (i.e., gravitational shear) no longer works because of the lack of background sources.

This is illustrated in Fig. 8, which shows the mass sensitivity of PICO using a spatial filter optimized for extracting the mass of halos [41]. The curves give the one-sigma noise in a mass measurement through the filter as a function of redshift. Their flattening at high redshift reflects the fact that CMB lensing is sensitive over a broad range of redshifts, extending well beyond the limit of $z = 2$ of the figure. We see that PICO can measure the mass of individual low-mass clusters ($\sim 10^{14} M_\odot$) over a wide redshift range, and by stacking we can determine the mean mass of much smaller halos, including those hosting individual galaxies.

Halo lensing will enable use to calibrate the galaxy cluster mass scale critical for our cosmological analysis of PICO cluster counts. It also gives us a unique tool for measuring the relation between galaxies and their dark matter halos during the key epochs of cosmic star formation at $z \geq 2$, not reachable by other means. This will provide valuable insight into the role of environment on galaxy formation during the rise to and fall from the peak of cosmic star formation at $z \sim 2$. **wasn't there an point about foreground cleaning for higher resolution experiments?**

Gravitational Lensing as Noise for Gravity Wave Science

does this belong here or in gravity waves? One of the most pronounced effects of lensing is the

emergence of the ‘lensing B-mode power spectrum’, which is a result of gravitational lensing of E -modes into B -modes; see Figure ???. reference figure in fundamental physics? When the tensor to scalar ratio $r \simeq 0.01$, the B-mode lensing power spectrum and the one from gravity waves have approximately the same level at $\ell = 80$, which is the angular scale at which the inflationary BB spectrum peaks. For lower levels of r , this peak is masked by E -mode photons that are lensed into B . But the B -mode maps can be ‘delensed’ [36, 37]. The effect of lensing on E and B maps can be determined and undone if these maps are measured with few arcmin resolution and with sufficient depth. Forecasts for PICO show that at a minimum 73% of the lens-induced B -mode power will be removed for the ‘requirement’ configuration, after accounting for foreground subtraction. 80% will be removed if the foregrounds do not degrade the inherent SNR, rising to 85% for the CBE. Without delensing PICO determination of r would be limited to $r > ??$. We emphasize that PICO will be relying on its own data to conduct the delensing and foreground cleaning, thus avoiding reduced efficacy arising from the need to cross-calibrate experiments, identify common observing areas on the sky, not having frequency band coverage at the appropriate resolution to remove foregrounds, or from other systematic uncertainties.

Physics of Galaxy Formation via the Sunyaev-Zel’dovich (SZ) Effects

Not all CMB photons propagate through the universe freely; about 6% are Thomson-scattered by free electrons in the intergalactic medium (IGM) and intracluster medium (ICM). These scattering events leave a measurable imprint on CMB temperature fluctuations, and they contain a wealth of information from how structure grows to the thermodynamic history of baryons. A fraction of these photons are responsible for the Sunyaev–Zel’dovich effects [? ?]. The thermal SZ effect (tSZ) is the increase in energy of CMB photons due to scattering off hot electrons. This results in a spectral distortion of the CMB blackbody that corresponds to a decrement in CMB temperature at frequencies below 217 GHz and an increment at frequencies above. The kSZ effect is the Doppler shift of CMB photons Thomson-scattering off free electrons that have a non-zero peculiar velocity with respect to the CMB rest frame. The amplitudes of the tSZ and kSZ signals are proportional to the integrated electron pressure (tSZ) and momentum (kSZ) along the line of sight, respectively. They thus contain information about the thermodynamic properties of the IGM and ICM. The tSZ effect can be used to measure ensemble statistics of galaxy clusters, which contain cosmological information, as well as to provide uniform cluster samples for galaxy formation studies in dense environments.

Galaxy Clusters

Galaxy clusters found via the tSZ effect provide a well-defined sample with a simple-to-model selection function. Sample of clusters such as these are easy to use for cosmological inferences and studies of galaxy evolution in dense environments. Points to still hit. High z sample, Numbers – Nick and Jim should cross-check, most massive cluster all over the whole sky, Cosmology.

Compton-y map and tSZ auto-power spectrum

In addition to finding individual clusters, multifrequency CMB data also allow the reconstruction of full-sky maps of the thermal SZ signal (Compton-y maps) via foreground removal algorithms similar to those used to obtain cleaned maps of the CMB. With its extremely low noise and broad frequency coverage, PICO will yield a definitive Compton-y map over the full sky, with high S/N down to angular scales of a few arcminutes. We quantify this expectation by reconstructing the Compton-y field using the needlet internal linear combination (NILC) algorithm [?] applied to sky simulations generated with the *Planck* sky model, with maps at all PICO frequencies (with appropriate noise added). The error bars on the reconstructed tSZ power spectrum are shown in

Fig. 9, in comparison to current measurements. The total $S/N = 1270$ for the PICO CBE configuration, with the PICO requirements configuration only $\approx 10\%$ lower. This is nearly two orders of magnitude larger than the current S/N from *Planck*.

Extremely strong constraints on models of astrophysical feedback will be obtained from the analysis of the PICO y -map, both from its auto-power spectrum and from cross-correlations with galaxy, group, cluster, and quasar samples [did we say what is feedback?](#). Like the CMB lensing map described above, the legacy value of the PICO y -map will be immense. As an example, we forecast the detection of cross-correlations between the PICO y -map and galaxy weak lensing maps constructed from LSST and WFIRST data. Considering the LSST “gold” sample with a source density of 26 galaxies/arcmin² covering 40% of the sky, we forecast a detection of the tSZ – weak lensing cross-correlation with $S/N = 3000$. At this immense significance, the signal can be broken down into dozens of tomographic redshift bins, yielding a precise breakdown of the evolution of thermal pressure over cosmic time. For PICO and WFIRST (assuming 45 galaxies/arcmin² covering 5.3% of the sky), we forecast $S/N = 1100$ for the tSZ – weak lensing cross-correlation. The WFIRST galaxy sample extends to higher redshift, and thus this high-S/N measurement will allow the evolution of the thermal gas pressure to be probed to $z \approx 2$ and beyond, the peak of the cosmic star formation history. These transformative measurements will revolutionize our understanding of galaxy formation and evolution by distinguishing between models of feedback energy injection at high significance. Additional cross-correlations of the PICO y -map with quasar samples, filament catalogs, and other large-scale structure tracers will further demonstrate its immense legacy value.

2.2.3 Galactic Structure and Star Formation (3 pgs, Chuss & Fissel)

Introduction

Cosmic magnetism is an outstanding puzzle of fundamental importance to astrophysics. Magnetic fields are ubiquitous, and their evolution is critically interwoven with the dynamics of the universe. Hence, it is crucial to understand their origin and the dynamo processes that must have amplified weak primordial seed fields and maintained their strength across cosmic time [45]. As often in astrophysics, our understanding is rooted in observations of the very local universe: the Milky Way and nearby galaxies. Magnetic fields are observed to be a foremost agent of the Milky Way’s ecology. They hold keys for making progress on some exciting issues in the astrophysics of galaxies: the dynamics and energetics of their multiphase interstellar medium (ISM), the efficiency of star formation, the acceleration and propagation of cosmic rays and the impact of feedback on their evolution. Magnetic fields are not only critical for understanding galaxies. The magnetized ISM in the Solar Neighborhood presents a challenge for the investigation of cosmological signals. Dust and synchrotron emission from the Galaxy hampers measurements of CMB polarization and spectral distortions. The Galactic ISM hinders investigation of the 21cm line emission of neutral hydrogen from cosmic dawn and the epoch of the Universe reionization, as well as of extragalactic magnetic fields.

A broad range of science topics call for progress in our modeling of Galactic magnetic fields, which in turn motivates ambitious efforts to obtain relevant data. As a result, today Galactic magnetism is a dynamic research field, driven by major advances in observational capabilities.

Observations of Galactic polarization are a highlight and a lasting legacy of the *Planck* space mission. Spectacular images combining the intensity of dust with the texture derived from polarization data have received world-wide attention and have become part of the general scientific

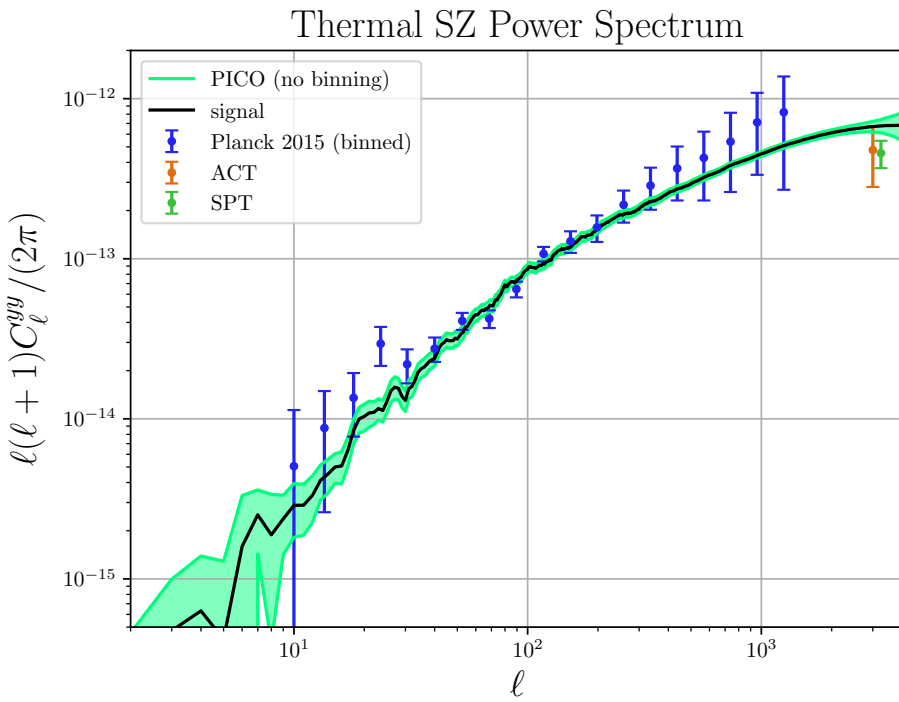


Figure 9: Constraints on the tSZ power spectrum from PICO and current data. The black curve shows the simulated tSZ power spectrum signal. The light green shaded region shows the error bars for PICO at each multipole, i.e., with no binning, as determined from NILC analysis of full-sky simulations. The blue points show the current constraints from Planck, which have been averaged into broad multipole bins. The orange and dark green points show the constraints from ACT and SPT, respectively, at a single multipole of $\ell = 3000$. The overall PICO $S/N = 1270$, nearly two orders of magnitude larger than current measurements.

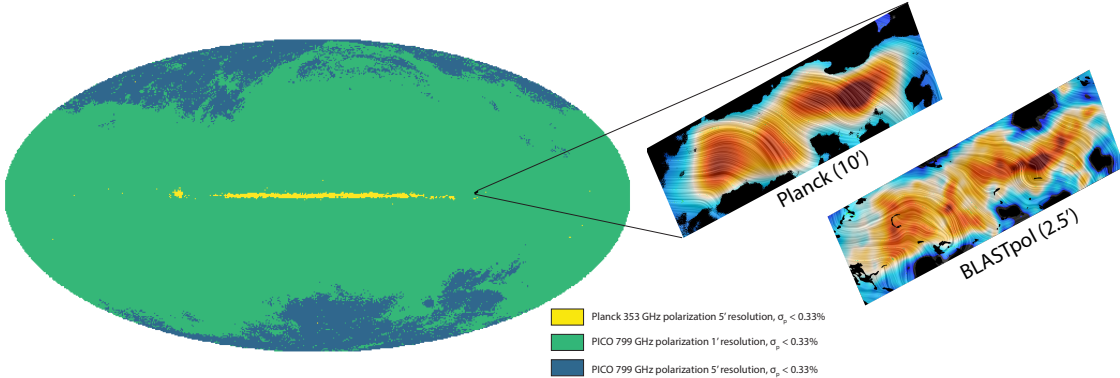


Figure 10: At 799 GHz, PICO will map nearly the entire sky at 1' resolution. As an example of the current state-of-the-art, Planck (10') and BLASTpol (2.5') maps of the Vela C region are shown [47]. These observations will enable PICO to characterize magnetized turbulence from the diffuse ISM down to dense star forming cores.

culture [46]. Beyond their popular impact, the Planck polarization maps represented an immense step forward for Galactic astrophysics (Planck Results 2018 XII). We expect an even greater leap forward from PICO as already hinted at by the higher angular resolution dust polarization images obtained with the balloon experiment BLASTPol. PICO will provide all-sky maps of dust polarization at sub-mm wavelengths, far deeper than that of Planck at 353,GHz, which can uniquely be obtained from a space mission. Planck made hundreds of thousands of measurements of magnetic field orientation across the sky; with PICO we expect 150 million independent measurements in just one frequency band. The data will complement a rich array of polarization observations including stellar polarization surveys to be combined with Gaia astrometry and synchrotron observations measuring Faraday rotation at radio wavelengths with the Square Kilometer Array and its precursors. In this section we focus on three key crucial Galactic science measurements that only PICO can obtain.

(1) *Testing Composition Models of Interstellar Dust:* The analysis of the PICO data will involve the spectral characterization of Galactic polarization. This aspect of the data analysis will contribute to update and test models of dust emission and of grain alignment, which are of interest for the interpretation of dust polarization data at large.

(2) *Determining how magnetic fields affect the process molecular cloud and star formation:* Because dust emission traces dust mass, and since the interstellar dust and the gas are dynamically coupled, dust polarization probes magnetic fields in the cold and warm neutral phases of the ISM and in molecular gas. If the magnetic fields are sufficiently strong, they can prevent the gravitational collapse of gas across magnetic field lines and can slow down or limit the process of star and planet formation. In the diffuse ISM the neutral phase of the interstellar medium contains the bulk of the gas mass and of its turbulent kinetic energy. Thus, PICO is best suited to study the dynamical interplay between gravity, turbulence, and magnetic fields in the ISM.

Dust Physics

Strong extinction features at 9.7 and 18 μm indicate much interstellar dust is in the form of amorphous silicates while features at 2175 Å, 3.3 μm , and 3.4 μm attest to abundant hydrocarbons. It is unknown, however, whether the silicate and carbonaceous materials coexist on the same grains or whether they are segregated into distinct grain populations. If there are indeed multiple grain

species, this will induce additional challenges for modeling the emission from interstellar dust in both total intensity and polarization at levels relevant for B-mode science [48].

Spectropolarimetry of dust extinction features found robust polarization in the $9.7\text{ }\mu\text{m}$ silicate feature [e.g., 49], indicating that the silicate grains are aligned with the interstellar magnetic field. In contrast, searches for polarization in the $3.4\text{ }\mu\text{m}$ carbonaceous feature have yielded only upper limits, even along sightlines where silicate polarization is observed [50, 51]. These data suggest that most of the silicate and carbonaceous materials do not exist on the same grains. However, these studies are limited to only a few highly-extincted sightlines that may not typify the diffuse ISM.

At odds with the spectropolarimetric evidence from dust extinction, current measurements of the polarization fraction of the far-infrared dust emission with *Planck* [52] and BLASTPol [53] betray little to no frequency dependence, as would be expected if two components with distinct polarization properties were contributing to the total emission. However, current uncertainties are relatively large and the data with $\nu > 353\text{ GHz}$ are from high density sightlines that may not be representative of the diffuse ISM. With great polarization sensitivity even in diffuse regions, PICO will provide a definitive test of the two component paradigm.

To assess PICO’s ability to discriminate quantitatively, we employ the analytic two component dust model of [54] which provided a better fit to IRAS and *Planck* data than one component models.

Applying the noise estimates from PICO, 1000 simulations were run for different combinations of polarization fractions of the two components in this model. Only frequency channels 107 GHz and above were used, and the simulated data were binned to the $7.9'$ beam of PICO’s 107 GHz channel. Based on the variance of the simulation results, PICO can determine the intrinsic polarization fractions of the two components to a precision of 1-2%. PICO will therefore be able to validate or reject state-of-the-art dust models [e.g. 55, Hensley & Draine, in prep] and test for the presence of additional grain species with distinct polarization signatures, such as magnetic nanoparticles [56].

Are Magnetic Fields Responsible For Low Star Formation Efficiency?

Stars form out of dense, gravitationally unstable regions within molecular gas clouds. The efficiency of this conversion from molecular gas to stars is very low, due to regulation from supersonic turbulent gas motions, magnetic fields, and feedback from young stars [57]. Magnetic fields may play an important role in slowing the process of star formation by inhibiting movement of gas in the direction perpendicular to the field lines. Observations to date suggest that the outer envelopes of clouds can be supported against gravity by magnetic fields, but in dense cores gravity tends to dominate, and so these dense structures can collapse to form stars [58].

On larger scales, the formation of gravitationally unstable clouds is regulated by the flow of diffuse material into the molecular phase, a process that is mediated by magnetized turbulence in the low-density ISM. Structure formation in the diffuse ISM is poorly understood, but as a precursor to star formation it is crucial to understand what drives molecular cloud formation. Recent observations suggest that the structure of the diffuse medium is highly anisotropic, and strongly coupled to the local magnetic field [59, 60, 61, 62].

However, the degree to which magnetic fields affect the formation of molecular clouds as well as stars within these clouds is poorly constrained, in large part due to the difficulty of making detailed maps of magnetic fields in the interstellar medium.

Formation of Stars within Magnetized Molecular Clouds

With full-sky coverage and a best resolution of $1.1'$ PICO will be able to map all molecular clouds

with better than 1 pc resolution, out to a distance of 3.4 kpc. Extrapolating from the Bolocam Galactic Plane Survey [BGPS, 63], we expect PICO to make highly detailed magnetic field maps of over 2,000 molecular clouds with thousands to hundreds of thousands of independent measurements per cloud.

Our goal is to constrain both the strength of the magnetic field, B , within these clouds, as well as the energetic importance of the field compared to self-gravity (parameterized by the mass-to-flux ratio μ) and turbulence (parameterized by the Alfvén Mach number M_A) as a function of density. To measure these quantities we will apply a series of established polarization analysis techniques: (1) characterizing the relative orientation of cloud structures and the magnetic field [64, 65, 66, 67]; (2) probability distributions functions of polarization measurables [47, 68]; (3) comparison between the magnetic field and velocity gradient directions [69, 70, 71]; and (4) measuring the angular dispersion of the magnetic field [72, 73, 74, 75]. By applying all four techniques to both PICO observations and synthetic polarization maps made from “observing” numerical simulations of star formation, we will quantitatively compare theory and observations. PICO’s large number of frequency bands will be used to better modeling the temperature and polarization efficiency of the cloud dust [76], which can then be used to generate more realistic generation of synthetic observations from simulations for comparison with PICO observations [77]. We can then compare the observed magnetization levels derived from the PICO observations to the levels of turbulence derived from molecular gas surveys (e.g.: (**author?**) 63, 78), and the efficiency of star formation, measured from near and far-IR observations of dense cores and protostars with *Herschel*, *Spitzer*, and *WISE*.

PICO’s ability to map thousands of clouds is not possible with any other current or proposed polarimeter. *Planck*, for example, was only able to map 10 nearby clouds to a similar level of detail [67]. This large sample of clouds is crucial because dust polarization observations are sensitive to only the magnetic field projected on the plane of the sky, and therefore polarization maps will look very different for molecular clouds observed at different viewing angles. **By observing thousands of molecular clouds PICO will determine the role of magnetic fields in star formation as a function of cloud age and mass.**

Formation of Magnetized Molecular Clouds from The Diffuse Interstellar Medium

Structure formation in the diffuse ISM is a key area of study motivating observations across the electromagnetic spectrum. PICO’s observations will complement recently completed high dynamic range neutral hydrogen (HI) surveys, such as HI4PI [79] and GALFA-HI [80], as well as planned surveys of interstellar gas, most prominently with the Square Kilometer Array (SKA) and its pathfinders. One of the open questions in diffuse structure formation is how gas flows within and between phases of the ISM. A planned all-sky absorption line survey with SKA-1 will increase the number of measurements of the ISM gas temperature by several orders of magnitude [81]. Quantitative comparisons of the ISM temperature distribution from SKA-1 and estimates of the magnetic field strength and coherence length scale from PICO will elucidate the role of the magnetic field in ISM phase transitions.

Despite its importance, a comprehensive understanding of the magnetized diffuse ISM is challenging because of its diverse composition, its sheer expanse, and the multi-scale nature of the physics that shapes it. How are matter and energy exchanged between the diffuse and dense media? This question must be addressed by measuring the properties of the magnetic field over many orders of magnitude in column density. PICO is unique in its ability to do this in the diffuse ISM. *Planck* achieved measurements of the diffuse sky at 60' resolution, resulting in \sim 30,000 in-

dependent measurements of the magnetic field direction in the diffuse ISM. With $1.1'$ resolution PICO will expand the number of independent polarization measurements in the diffuse ISM to $\sim 86,000,000$. This will allow us to robustly characterize turbulent properties like M_A across a previously unexplored regime of parameter space.

Legacy Science

PICO will also produce legacy datasets that will revolutionize our understanding of how magnetic fields influence physical processes ranging from planet formation to galaxy evolution. For 10 nearby clouds ($d < 500$ parsecs) PICO will resolve magnetic fields on the crucial 0.1 pc size scale associated with dense cores and filaments, and observe how the magnetic fields on these scales directly influence the formation structure of cores. By comparing the orientation of the core-scale magnetic field with respect to the orientation and sizes of protoplanetary disks, PICO will directly test whether there is evidence that magnetic breaking inhibits the growth of protoplanetary disks [82, 83].

On larger scales PICO’s tens of millions of independent measurements of magnetic field orientation from will allow us to directly probe magnetized turbulence with in unprecedented detail, allowing us to study how magnetic fields are generated through turbulence and large scale gas motions [84]. The magnetization levels of the also dramatically change key processes in the diffuse ISM, including heat transport [85], streaming of cosmic rays [86], magnetic reconnection [87] etc.

Finally, PICO observations will create detailed magnetic field maps of approximately 70 nearby galaxies, with more than 100 measurements of magnetic field direction per galaxy. These observations will be used to study the turbulence on galactic scales, determine whether the magnetic fields of the Milky Way in the Diffuse ISM are consistent with other galaxies, and directly study how interaction between large scale magnetic fields, turbulence, and feedback from previous generations of star galaxy evolution and star formation efficiency.

For all of the science described in PICO will provide crucial large number statistics all-sky coverage, and will bridge the spatial scales covered by its predecessor *Planck* and high resolution ground based telescopes like ALMA.

2.3 Legacy Surveys (2 pgs, de Zotti)

Describe science that we get for free.

2.3.1 Point extragalactic sources in the PICO frequency range

As illustrated by the left panel of Fig. 11, at $\lambda \gtrsim$ few mm the dominant extragalactic population are blazars (flat-spectrum radio quasars, FSRQs, and BL Lacs), typically at $z \gtrsim 1$; the solid blue line shows an example. At shorter wavelengths dusty galaxies take over. The brightest sources in this spectral range are nearby star-forming galaxies like M 61. PICO will also see the brightest high- z sub-mm sources which, due to the “magnification bias”, are those whose flux density is boosted by strong gravitational lensing.

Herschel surveys have shown that, at $500\mu\text{m}$ (600 GHz), about 20% of galaxies at the PICO detection limit are strongly lensed (right panel of Fig. 11). This is an extraordinary selection efficiency: for comparison, the fraction of strongly lensed galaxies is of $\sim 10^{-3}$ in all other frequency bands where searches have been carried out. Also, these galaxies have sub-mm colors substantially different from those of the other extragalactic populations and are therefore very easily singled out [89].

PICO will detect several thousands strongly lensed galaxies. Objects like the $z = 4$ source

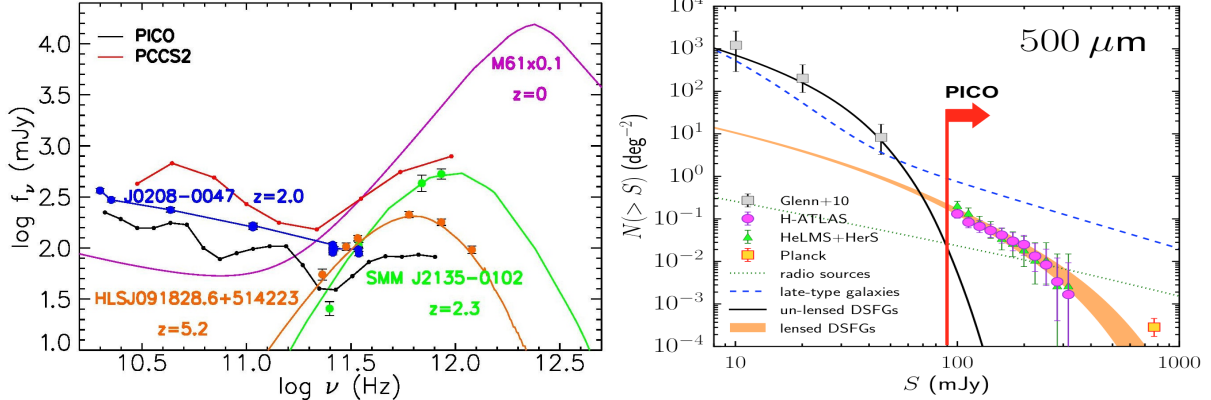


Figure 11: **Left panel.** Examples of SEDs of extragalactic sources detectable by PICO, compared with its point source detection limits (solid black line). The SED of M 61 has been scaled down by a factor of 10. The 90% completeness limits of the Second *Planck* Catalogue of Compact Sources (PCCS2; [88]) are also shown. **Right panel.** Integral counts of the various populations of extragalactic sources at $500\mu\text{m}$ as determined by *Herschel* surveys. The vertical red line shows the estimated PICO detection limit.

HLSJ091828.6 + 514223 (left panel of Fig. 11; [90]) would be detectable by PICO up to extreme redshifts ($z > 10$).

The availability of thousands of strongly lensed galaxies opens exciting prospects both on the astrophysical and on the cosmological side (cf., e.g., ref. [91]). Compared to searches in other wavebands, PICO detections will extend to much higher redshift sources [most optically-selected strongly lensed galaxies are at $z < 1$, cf. Fig. 7 of ref. 91] and will pick up the rare most extreme amplifications, thanks to its all sky coverage: the magnification factors, μ , of “*Planck* dusty GEMS” are estimated to be of up to 50 [92].

Sub-mm lensing allows us to probe the most active star-formation phases, hardly visible in the optical. The gravitational flux boosting is accompanied by a stretching of images. Thus follow-up with ALMA can achieve an effective resolution of several milli-arcsec, i.e. can measure galactic structures at $z \simeq 3$ down to the astounding level of $\sim 50 - 60\text{pc}$, much smaller than the sizes of Galactic giant molecular clouds [93]. This provides unique direct information on the mechanisms driving the star-formation and on the shapes, sizes and surface brightnesses of star-formation regions.

The detection of several thousands of galaxies at redshifts $\gtrsim 1$ and up to $z > 5$ allows a substantial progress towards a complete census of the dust-enshrouded star-formation history of the universe, i.e. towards tracking the buildup of stellar mass over cosmic time, in particular over epochs of most intense star formation.

The high redshifts of magnified galaxies imply high redshifts of foreground lenses. Optical follow-up will allow us to investigate the total (visible and dark) mass of the lensing galaxies, their density profiles, dark matter sub-structures in a much higher redshift range than in the case of optical selection [94].

Also PICO will explore essentially the entire Hubble volume for the most intense hyperluminous starbursts, testing whether there are physical limits to the star-formation rates of galaxies.

The right panel of Fig. 11 also shows that PICO will detect tens of thousands star forming galaxies in the nearby universe, reaching a surface density about a factor of two higher than that of the

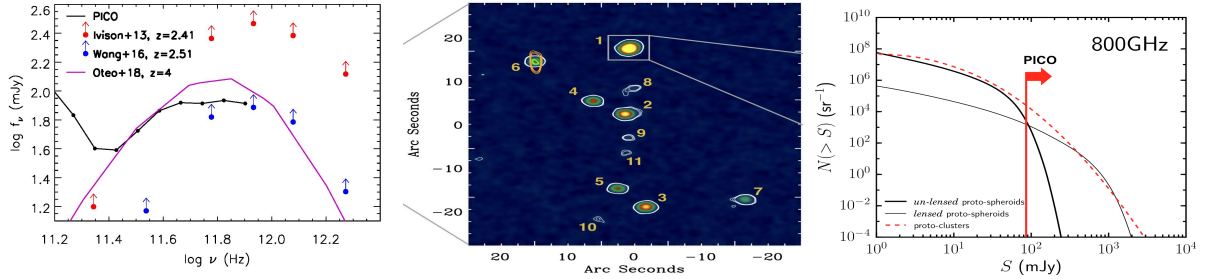


Figure 12: **Left panel.** SEDs of the cores of two proto-clusters of starbursting galaxies discovered by [97] at $z = 2.41$, by [98] at $z = 2.506$ and by [99] at $z = 4.0$. The first two SEDs include only the contributions of proto-cluster members within $10''$, i.e. over an angular size below the PICO resolution, corresponding to physical radii $\simeq 80$ kpc, substantially smaller than the effective proto-cluster sizes. The reported flux densities are therefore lower limits to those that will be measured by PICO. The SED of the $z = 4.0$ proto-cluster correspond to a SFR of $6500 M_\odot \text{yr}^{-1}$, estimated by [99] summing the contributions of galaxies detected by ALMA within a radius of $\simeq 25''$; again this is likely a lower limit to what PICO will measure. The solid black line shows the PICO detection limits. **Central panel.** ALMA image of the $z = 4.0$ proto-cluster discovered by [99], extracted from Fig. 1 of their paper. **Left panel.** Counts of proto-clusters at 800 GHz predicted by the model of ref. [100]. The vertical red line corresponds to the PICO detection limit.

IRAS satellite at its $60\mu\text{m}$ completeness limit [95]. The IRAS wavebands are relatively insensitive to low temperature dust emission, a significant and largely unexplored component of many nearby galaxies [96]. PICO will provide a full characterization of this component, complementing IRAS data to establish well calibrated dust SEDs as a function of galaxy morphology, luminosity, dust and gas mass, etc..

2.3.2 Early phases of cluster evolution

PICO will open a new window for the investigation of early phases of cluster evolution, when their member galaxies were actively star forming and before the hot IGM was in place. In this phase traditional approaches to cluster detection (X-ray and SZ surveys, searches for galaxy red sequences) work only for the minority of evolved objects; indeed they have yielded only a handful of confirmed proto-clusters at $z \gtrsim 1.5$ [101]².

SEDS of spectroscopically confirmed sub-mm-bright proto-clusters detectable by PICO are shown in the left panel of Fig. 12. *Planck* has demonstrated the power of low-resolution surveys for the study of large-scale structure [102] but its resolution was too poor to detect individual proto-clusters [100]. As illustrated by the central panel of Fig. 12, the typical sizes of high- z proto-cluster cores are of $\sim 1'$ (cf. also ref. [103]), nicely matching the PICO FWHM at the highest frequencies.

CMB Probe will detect many tens of thousands of these objects (right-hand panel of Fig. 12) up to $z \gtrsim 4$ (left panel). This will allow a real breakthrough in the observational validation of the formation history of the most massive dark matter halos, traced by clusters, a crucial test of models for structure formation. Follow-up observations will characterize the properties of member galaxies, probing the galaxy evolution in dense environments and shedding light on the complex physical processes driving it.

²More high- z proto-clusters have been found targeting the environment of tracers of very massive halos, such as radio-galaxies, QSOs, sub-mm galaxies. These searches are however obviously biased.

2.3.3 Radio sources

PICO will increase by orders of magnitude the number of blazars selected at sub-mm wavelengths and will determine the SEDs of many hundreds of them up to 800 GHz. The most luminous high- z FSRQs were found to host black holes (BHs) with the largest masses, up to $\sim 4 \times 10^{10} M_{\odot}$ (S50014+813, at $z = 3.366$; see ref. [104]). Such objects have particularly hard mm-wave spectra; thus PICO surveys are well suited to detect them. Objects like S50014 + 813 are detectable by PICO up to $z > 5$.

Blazar searches are the most effective way to sample the most massive BHs at high z because of the Doppler boosting of their flux densities. Since the flux boosting occurs for jets closely aligned with the line of sight ($\theta < 1/\Gamma$, $\Gamma \sim 15$ being the bulk Lorentz factor), for each FSRQ there are other $2\Gamma^2$ (i.e. hundreds) sources of similar intrinsic properties but pointing elsewhere.

Very large BH masses at high- z challenge models because it is very hard to grow a seed BH from stellar mass to $> 10^9 M_{\odot}$ in the limited age of the universe. It is even more so for jetted quasars because jets are likely associated with rapidly spinning BHs whose radiative efficiency is large so that the mass growth is slow. Yet at least 4 FSRQs has been discovered at $z > 5$ (up to $z = 5.48$; [105]). One (SDSS J013127.34032100.1 at $z = 5.18$) has estimated BH mass of $\sim 10^{10} M_{\odot}$ [106].

The PICO surveys of the largely unexplored mm/sub-mm spectral region will also offer the possibility to discover new transient sources [107] or events, such as blazar outbursts.

2.3.4 Source polarization

PICO will make a giant leap forward in the determination of polarization properties of both radio sources and of dusty galaxies over a frequency range where ground based surveys are impractical or impossible. Thanks to its high sensitivity, it will detect in polarization both populations over a substantial flux density range, determining directly, for the first time, number counts in polarized flux density.

Mm/sub-mm polarimetry of radio sources provides unique information on the magnetic field configuration (geometry and degree of order) in the innermost, unresolved regions of the jets, close to the active nucleus. Polarimetry of dusty galaxies as a function of their inclination is informative on the structure and on the ordering of their large-scale magnetic fields.

2.4 Complementarity with Other Surveys and with Sub-Orbital Measurements (1 pg, Lawrence, Schmittfull)

Should describe complementarity with other astrophysics surveys (both space and ground) and with sub-orbital CMB measurements. For the astrophysical surveys, this is summary text of text that is presumably sprinkled elsewhere in the proposal; please cross-reference.

2.4.1 Complementarity with Astrophysical Surveys in the 2020s

For cosmological constraints on the sum of neutrino masses, there is no known way to achieve $\sigma(\sum m_{\nu}) < 25 \text{ meV}$ without improving measurements of the optical depth τ over *Planck*'s low- ℓ polarization constraint (see the neutrino mass section above). In particular, this applies to all methods that rely on comparing low-redshift structure with the amplitude of the CMB at high redshift, such as galaxy clustering, weak lensing, or cluster counts. (Should add a sentence on ongoing work that attempts to get around τ : still not possible to do better than 25meV even with LSST and CMB-S4.) Improving τ and therefore $\sigma(\sum m_{\nu})$ is only possible by improved observations of low- ℓ E modes, which are only possible from space. With its improved τ measurement PICO would

Characteristic	Ground	Balloon)	Space
Sky coverage	Partial from single site	Partial from single flight	Full
Frequency coverage	Limited atmospheric windows. $\nu = 70$ GHz inaccessible. $\nu \geq 300$ GHz unusable.	Better than ground. $\nu = 70$ GHz	Unrestricted
Angular resolution	$1'$ resolution possible	$\gtrsim 4'$ possible	$\gtrsim 6'$ possible
Detector Noise	$\geq xx$ microK rt(s); atmospheric 1/f noise requires subtraction	$\geq xx$ microK rt(s)	xx microK rt(s)
Integration time	Limited by Sun, weather	Limited by Sun, flight duration	Continuous, for years.
Accessibility, repairability	Good	None. Multiple flights possible.	None.

Table 2: Caption

therefore directly improve neutrino mass constraints when combined with late-time probes, reaching $\sigma(\sum m_\nu) < 15$ meV. PICO therefore complements all efforts that probe the late time structure of the Universe to constrain the sum of neutrino masses, and combining PICO with these low-redshift observations enables more than any cosmological experiment could achieve on its own.

Reconstructing the CMB lensing convergence on very large angular scales, $L_K < 20$, requires exquisit systematics control over a large sky fraction as well as high angular resolution to perform the lensing reconstruction. A space mission like PICO would provide that, complementing ground-based CMB lensing reconstructions that typically observe smaller sky fraction (or at least have different observation noise in different areas of the sky due to scanning strategy), which makes it difficult to reconstruct lensing on the largest scales. Indeed, PICO could robustly measure the lensing signal with a power spectrum signal-to-noise ratio of more than 100 per mode on very large scales (based on Alex Van Engelen noise plot from PICO meeting; is this still up to date?). Such high-significance CMB lensing measurements on the very largest scales can be useful when combined with measurements of galaxy clustering to search for local primordial non-Gaussianity via its scale-dependent effect on galaxy bias. In an idealized forecast, we find $\sigma(f_{NL}) \simeq 0.5$ for $L_{\min}^{KK,Kg,gg} = 4$, and $\sigma(f_{NL}) \simeq 0.9$ for $L_{\min}^{KK,Kg,gg} = 20$, assuming optimistic LSST galaxy clustering with 60arcmin^{-2} galaxies and with high-redshift dropout galaxies. This would be a notable improvement over the best current constraint $\sigma(f_{NL}) = 5$ from *Planck*. Such a measurement would ultimately likely be limited by limitations of LSST on the very largest scales, but space based observations of galaxy clustering with Euclid or SPHEREx could help in this regard.

2.4.2 Complementarity with Sub-Orbital Measurements

Since the first measurements that recognized the existence of the CMB were made in 1964, important observations have been made from the ground, from balloons, and from space. The question for the future is what should the roles be of these three types of experimental approaches? To answer this question, start by considering the advantages and disadvantages of each location (Table ?).

In every respect affecting performance, space has the advantage, and there can be no argument that space will be required to reach the ultimate limits set by astronomical foregrounds. But the advantages of space come at a high cost, in both time and money, and an essential question is how much can be done from the ground and balloons first? The answer depends on the specific requirements of the science questions being addressed, which we discuss below. However, some general guidelines can be given. When the entire sky is needed, as for fluctuations on the largest angular scales, space is necessary. The difficulties of controlling systematic errors and foregrounds over the whole sky at a level significantly below what has been achieved by *Planck* are simply too great to overcome on the ground. Progress on the reionization bump ($2 \leq \ell \leq 12$), whether for τ or for r , requires space. Significant progress can surely be made from the ground on the recombination

bump ($30 \leq \ell \leq 300$), and the $r \approx 10^{-3}$ goal of the “ultimate” ground-based experiment CMB-S4 looks to be both bold and achievable. For r , the confusing signal from large-scale-structure lensing of CMB E -modes into B -modes must be measured and removed, and this requires observations on sub-degree scales over a wide frequency range (because of foregrounds) that especially at the lower frequencies is a challenge from space.

The PICO r goal of 10^{-4} is beyond the reach of ground observations. The limited frequency range observable from the ground is not enough to separate foregrounds to the necessary level, and at 10^{-4} there is no room to give up any advantage on systematics. For science requiring higher angular resolution, however, such as observations of galaxy clusters at 1 arcmin resolution, the ground has a clear advantage.

(need more in here)

Balloon observations have been valuable in the past, but the severe limitations on observing time must be recognized. Even the ultra-long-duration balloons that have been on the horizon for more than two decades but have not yet flown for any astrophysics experiment offer only 10^2 days per flight, 5–10% of the duration of the Planck mission (depending on instrument), and 3% of the duration of WMAP. Both WMAP and Planck showed the essential power of repeated observations in identical conditions in revealing and controlling systematics. This will never be possible with balloon experiments. Reaching 10^{-4} will require vigorous exploitation of *every* possible advantage. There is nevertheless still an important role for balloon experiments, in demonstrating new technologies, and in training of students.

2.5 Signal Separation (4 pgs, Jacques and Clem)

Enumerate the various signals in polarization. Use the frequency band + signals figure. The challenge is to dig out the faintest of all signals, the one due to r . This sets the tone for the entire ‘signal decomposition’ or ‘component separation’. Removing the galactic signal to unmask $r \lesssim 0.001$ is a challenge for all future experiments searching for r at that level, and is a strong advantage of a space platform. The physics of galactic signals suggests complexities in their combined emission properties; the level of this complexity is not known.

Contamination of CMB observations by astrophysical foreground emission of various origins is one of the major challenges that future observations of CMB polarization must face. Polarized emission in the PICO frequency range is known to be dominated by synchrotron emission from the galactic interstellar medium in our own galaxy and by thermal emission from interstellar dust. Although much has been learnt about these polarized foregrounds with WMAP and Planck observations, their exact properties are not known at the level that would be needed to guarantee that they can be separated out from the CMB using known component separation techniques. In particular neither the exact form one should assume for the frequency scaling of their emission (if any), nor the variation of these emission laws across the sky or along the line of sight, nor the small-scale distribution of emission, are known at the required level of detail. Whether other processes emit at a level that can contaminate PICO observations significantly is also not known at present.

The many frequency channels of PICO can be used to learn from the PICO observations themselves the properties of these foregrounds, and to identify the CMB contribution in the multifrequency data using its unique spectral signature. To be robust against our uncertainty about the foregrounds, we assess the feasibility of foreground cleaning for different models of foreground emission of varying complexity, from optimistic to pessimistic, and for various component separation methods.

To assess the performance of PICO we have carried out map based simulations within a “data challenge” framework. In this process one group prepares sets of simulated maps which are placed in a shared area. These are then re-analyzed by multiple individuals and groups employing various different component separation algorithms.

2.5.1 PICO Map Based Simulations

For the CMB we take realizations of lensed- λ CDM shared from the Planck FFP10 simulation set. For the noise we take white noise realizations with the appropriate levels at each of the 21 bands. For the foregrounds we use a suite of 3rd party models:

- **00:** Simple Gaussian realizations of synchrotron and dust with power-law angular power spectra at amplitudes set to match the observations in the BICEP/Keck field, and simple uniform SEDs (power law for synchrotron, greybody for dust).
- **01:** The PySM³ model `a1d1f1s1`, where the letters refer to anomalous microwave emission, dust, free-free and synchrotron respectively, and the numbers are the base models described in [108].
- **02:** The PySM model `a2d4f1s3`, where the models have been updated to variants that are also described in [108]. Note that these include 2% polarized AME, a curvature of the synchrotron SED, and a two-temperature model for dust.
- **03:** The PySM model `a2d7f1s3`, where the dust model has been updated to a sophisticated physical model of dust grains as described in [109]. This model is interesting in that it does not necessarily conform to the greybody SED.
- **06:** A model based on MHD simulations [110] of the Galactic magnetic field, which naturally produces non-Gaussian correlated dust and synchrotron emission.
- **08:** A multilayer model of dust [111] which seeks to include the variation of the SED along the line of sight—i.e. in this model the behavior does not conform to a single greybody even within a high resolution pixel (as it will not in reality).
- **09:** A model of dust and synchrotron which implements non-Gaussian smaller scale structure and includes some decorrelation of the dust pattern as a function of frequency [112].

2.5.2 Needlet re-analysis

The NILC is based on Internal Linear Combinantion (or ILC in short) component separation method. It has been applied to the PICO simulations to determine the angular power spectrum of the B-mode polarized CMB signal. This method only attempts to reconstruct the CMB signal, without using any prior information about foregrounds. It is based on two specific assumptions. Firstly, that the CMB is frequency independent in thermodynamic unit, and secondly, that the CMB is uncorrelated with foreground signals. The ILC method then estimates the CMB, S_b, as a

³https://github.com/bthorne93/PySM_public

weighted linear combination of the set of input multi-frequency sky maps such that the variance of the estimate is minimum, with unit response to the flat CMB frequency spectrum,

$$\widehat{S} = w^T X = \frac{a^T \widehat{R}^{-1}}{a^T \widehat{R}^{-1} a} X = \frac{a^T \widehat{R}^{-1}}{a^T \widehat{R}^{-1} a} (aS + F + N), \quad (1)$$

where X is the vector of frequency maps, a the constant frequency spectrum of the CMB signal S , F the total foreground signal, N the instrumental noise for the different frequency channels, and R_b the frequency-frequency covariance matrix. The first condition guarantees minimum contamination by foregrounds and instrumental noise whereas the second condition guarantees that the CMB signal is conserved without bias. The presence of the foregrounds induces correlated errors across frequencies, so that the ILC weights adjust themselves to minimise the foreground residuals present in the the weighted linear combination. However, in reality the weights result from a trade-off between minimising the foregrounds and minimising the instrumental noise contribution in the reconstructed CMB map.

The ILC method can be straightforwardly implemented in either real (pixel) space or in harmonic space. Thus, sets of ILC weights can either be computed for different regions of the sky or for different angular scales, respectively, which allows for variations of the data covariance matrix in either space. However, the ILC in harmonic space does not take into account the fact that noise can be a significant source of CMB measurement error in at high Galactic latitude, while foreground signals are more important at low Galactic latitude. Conversely, the ILC in pixel space does not take into account the fact that the noise dominates on small angular scales, while diffuse Galactic foreground emission dominates on large angular scales.

In order to overcome this problem, we implement the ILC on a frame of spherical wavelets called needlets, a component-separation approach that we now refer to as the Needlet Internal Linear Combination (NILC) method. This technique has already been applied broadly in CMB data analysis. The needlets enable localised filtering in both pixel space and harmonic space because they have compact support in the harmonic domain, while still being very well localised in the pixel domain. The needlet decomposition allows the ILC weights to vary both smoothly on large angular scales and rapidly on small angular scales, which is not possible by sub-dividing the sky into different areas prior to any processing.

To analyse the simulations of sky for PICO, we have used 11 frequency channels (i.e. every alternate channels starting from the lowest frequency channel) and 11 needlet filters for the analysis. The needlet filters, h_l^j , in harmonic space that we use in our analysis are defined as follows,

$$h_l^j = \begin{cases} \cos \left[\left(\frac{l_{peak}^j - l}{l_{peak}^j - l_{min}^j} \right) \frac{\pi}{2} \right] & \text{for } l_{min}^j \leq l < l_{peak}^j, \\ 1 & \text{for } l = l_{peak}^j, \\ \cos \left[\left(\frac{l - l_{peak}^j}{l_{max}^j - l_{peak}^j} \right) \frac{\pi}{2} \right] & \text{for } l_{peak}^j < l \leq l_{max}^j \end{cases} \quad (2)$$

The simulated sky maps are first convolved or de-convolved in harmonic space to put them all at the same angular resolution (FWHM 15 arcmin) prior to the application of the NILC algorithm. Since the method as currently implemented is applicable to scalar fields on the sphere, sky maps of

Table 3: List of needlet bands used in the present analysis.

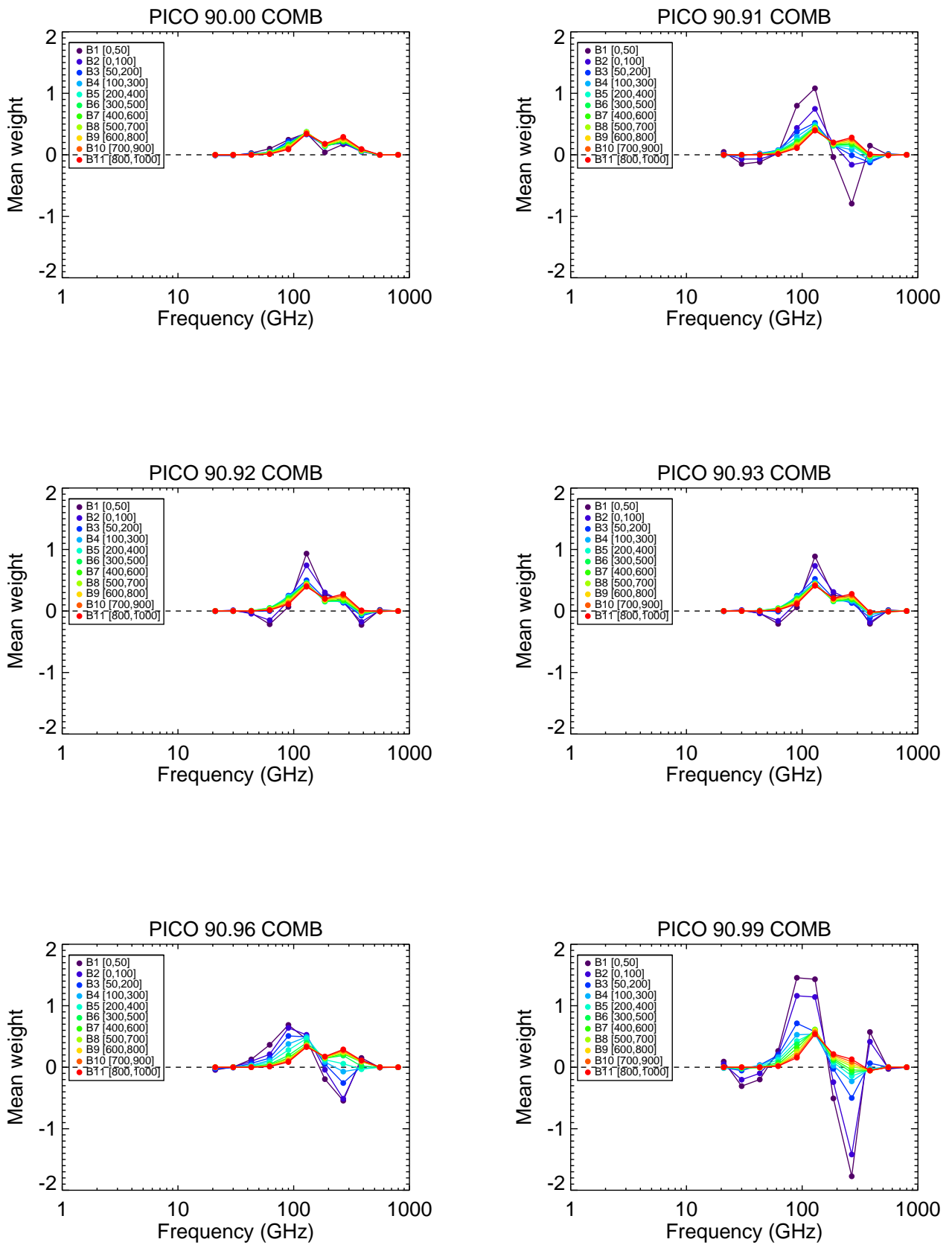
Band index	l_{min}	l_{peak}	l_{max}	nside
1	0	0	50	32
2	0	50	100	64
3	50	100	200	128
4	100	200	300	256
5	200	300	400	256
6	300	400	500	256
7	400	500	600	512
8	500	600	700	512
9	600	700	800	512
10	700	800	900	512
11	800	900	1000	512

the B modes are constructed from the input Stokes parameters, Q and U, on the full sky. The NILC weights used to combine the multi-frequency input data in order to estimate the CMB signal are then computed from the full-mission sky maps for B-mode. The derived weights are also applied to the half-mission maps, which are later used for minimising the impact of residuals of noise on the measurement of angular power spectrum.

The needlet weights are mostly determined by the galactic contamination, which dominates on large angular scales, and by the noise level, which dominates on small angular scales. Although the weights of for a subset of the frequency channels under consideration are relatively low compared to other channels, they are important for removing the Galactic foreground contamination. However, the reconstructed B-mode maps cannot be completely free from contamination by residual foregrounds and noise. Therefore, for further analysis, a set of conservative masks are derived from the residuals of foreground map. For the computation of the angular power spectrum of the high resolution NILC CMB maps, we use a pseudo-Cl estimator. Currently I am experimenting with different sets of confidence mask. Soon I will share with you the results obtained using those new mask.

2.5.3 PSM sky simulations at $N_{\text{side}} = 16$

The PSM (Planck Sky Model) [113] is a simulation software developed by the *Planck* Collaboration to model sky emissions at submillimetre to centimetre wavelengths based on the state-of-the-art observations of the *Planck* satellite mission and earlier surveys. We use the PSM to simulate all-sky polarization maps at the 21 frequency bands of *PICO* (21 to 800 GHz). The simulated components of emission include CMB E- and B-mode polarization, polarized Galactic synchrotron and thermal dust foreground emissions. The CMB template map is generated from CAMB [114] through CMB E- and B-mode power spectra by assuming an optical depth to reionization of $\tau = 0.06$ and a tensor-to-scalar ratio of $r = 10^{-3}$, as well as gravitational lensing effects. Galactic dust Q and U polarization maps are generated from the *Planck* GNILC dust intensity all-sky map at 353 GHz, in which cosmic infrared background (CIB), CMB, and noise have been filtered out, and assuming average polarization fractions of 5-10%. Galactic synchrotron Q and U



maps are based on the *WMAP* polarization observations at 23 GHz [115].

The thermal dust Q and U template maps are extrapolated across *PICO* frequencies through a modified blackbody energy spectrum having variable spectral index and temperature over the sky, using the Planck GNILC dust spectral index and temperature maps for which $\beta_d = 1.6 \pm 0.1$ and $T_d = 19.4 \pm 1.3$ K, respectively. The synchrotron Q and U template maps are extrapolated across *PICO* frequencies through a curved power-law spectrum, with a variable spectral index over the sky of $\beta_s = -3 \pm 0.06$ based on the synchrotron index map from [115], and a constant curvature of $C_s = 0.3$ [116] to account for different populations of cosmic ray electrons and possible AME polarization [117]. The CMB, dust, and synchrotron component maps in each *PICO* frequency are then co-added, and instrumental white noise is added to each sky map using the sensitivities per frequency quoted by *PICO*. The PSM simulations are generated at a pixel resolution of HEALPix [118] $N_{\text{side}} = 16$ ($2 \leq \ell \leq 47$), therefore assuming spectral variations of the foregrounds across $N_{\text{side}} = 16$ pixels.

2.5.4 PICO forecasts with COMMANDER

We have applied the COMMANDER algorithm [119] to the set of PSM $N_{\text{side}} = 16$ sky simulations for *PICO*. COMMANDER is a Bayesian parametric fitting method which has been thoroughly used by the *Planck* Collaboration for the separation of CMB and foreground components [120, 121]. Using MCMC Gibbs sampling in each pixel, the COMMANDER algorithm allows to fit simultaneously the amplitudes of CMB and foreground components, their spectral parameters, and the CMB E- and B-mode power spectra in a self-consistent Bayesian framework. A Blackwell-Rao estimator applied to the Gibbs samples allows in particular to reconstruct the statistical (chi-square) distribution of the CMB B-mode power spectrum at each multipole, and the posterior distribution of the tensor-to-scalar ratio [122, 123]. Such a Bayesian method performs end-to-end propagation of all foreground uncertainties towards the tensor-to-scalar ratio, while providing a chi-square goodness-of-fit in each pixel which allows to revise the parametric model or readjust the galactic mask a posteriori. The *PICO* sky maps are processed by COMMANDER using a Galactic mask leaving a 50% fraction of the sky, and forecasts on r are computed using the range of low multipoles $2 \leq \ell \leq 47$.

First considering *PICO* sky simulations *without foregrounds*, but just CMB and noise in the *PICO* frequency bands, we recover the tensor-to-scalar ratio with $\sigma(r = 10^{-3}) = 0.40 \times 10^{-3}$ significance: this provides the minimum uncertainty on $r = 10^{-3}$ that can be achieved by *PICO* from low multipoles $2 \leq \ell \leq 47$ in the absence of foregrounds on 50% of the sky. In the presence of foregrounds (full simulation), with variable spectral indices over the sky, the COMMANDER results on r are of similar quality due to the broad frequency range of *PICO* (21 -800 GHz), with $\sigma(r = 10^{-3}) = 0.41 \times 10^{-3}$ for *PICOv2-1.4* and $\sigma(r = 10^{-3}) = 0.36 \times 10^{-3}$ for *PICOv3* (increased sensitivities per channel) after foreground cleaning. Assuming now that 60% delensing in power has been achieved (modified PSM simulation with only 40% of the lensing B-mode power left in the CMB map realisation), the uncertainty on $r = 10^{-3}$ is improved by more than 30%, with $\sigma(r = 10^{-3}) = 0.24 \times 10^{-3}$ for *PICOv3* after foreground cleaning and 60% delensing. Finally, we note that discarding low- and high-frequency bands, resulting in a descoped version of *PICO* with a narrower frequency range of 43-462 GHz, the COMMANDER results are degraded by 75%, with an uncertainty increasing from $\sigma(r = 10^{-3}) = 0.4 \times 10^{-3}$ to $\sigma(r = 10^{-3}) = 0.7 \times 10^{-3}$ after foreground cleaning. The main reason for the degradation is a lack of constraining power on the dust temperature variations over the sky when discarding frequencies above 462 GHz, which translates

into a degradation of the fitted CMB B-mode power spectrum by extrapolation towards central frequencies.

[MR: I can add a figure on COMMANDER C_ℓ^{BB} results with *PICO*, if needed]

We are working in parallel on COMMANDER2, a new version of the algorithm operating in harmonic space, thus allowing to perform the parametric fit at full resolution and to further reduce the uncertainty on r by the increase of information / modes.

2.6 Systematic Errors (3 pgs, Crill)

Some of the PICO science goals attempt to reach extremely faint signals. The most ambitious one is to reach the nanoK-level signals characterizing an inflationary gravity wave with $r \lesssim 0.001$.
be more explicit about the level of the $\ell = 80$ peak It has long been recognized that exquisite control of systematic uncertainties will be required for any experiment attempting to reach these levels, and it is widely accepted that the stability provided aboard a space platform makes it best suited to control systematic uncertainties compared to other platforms. This is one of the most compelling reasons to observe the CMB from space. As WMAP? and *Planck* demonstrated, the L2 environment offers excellent stability as well as the ability to observe large fractions of the sky on many time scales without interference from the Sun, Earth, or Moon. The redundancy of observations allows the checking of consistency of results and an improved ability to calibrate and to correct systematic errors in post-processing analysis. there are several arguments here lumped in one sentence: suggest to make more explicit to PICO, and tie to the scan strategy. Also need to fold in the issue of 1/f (and absence of HWP.)

A rich literature investigates the types of systematic errors due to the environment, the instrumentation, observation strategies, and data analysis that confound the polarization measurement by creating a bias or an increased variance[124, 125, 126]. Every measurement to date has reached a systematic error limit, and have advanced many sophisticated techniques to mitigate systematics, finding both new technological solutions and new analysis techniques. As an example, the BICEP's systematics limited it to $r=0.1$ [?] while through additional effort within the program, BICEP2 achieved a systematics limit of $r=6 \times 10^{-3}$ [127]). In the near term, the ground based and suborbital CMB community will continue to develop new techniques in handling systematics, particularly in developing the CMB-S4 project.

All prior on-orbit measurements of CMB polarization were limited by systematic errors until an in-depth study of the systematics was performed and the post-processing data analysis suppressed them[10, 128, 129]. Particularly we note Fig. 3 of the *Planck* legacy paper which indicates *Planck*'s systematic error limits on the polarization power spectral measurements. Recently studied space missions, such as EPIC-IM, LiteBird and *CORE*, have placed systematic error mitigation at the forefront of the case for their mission and have developed tools and strategies for estimating and mitigating these[130, 131, 132].

Systematics are coupled with the spacecraft scan strategy, and the details of the data analysis pipeline. Thus, end-to-end simulation of the experiment is an essential tool, including realistic instabilities and non-idealities of the spacecraft, telescope, instrument and folding in data post-processing techniques used to mitigate the effects.

2.6.1 List of Systematics

The systematic errors faced by PICO can be categorized into three broad categories: 1) Intensity-to-polarization leakage, 2) stability, and 3) straylight, and are listed in Table 5. These were pri-

oritized for further study using a risk factor incorporating the working group's assessment of how mission-limiting the effect is, how well these effects are understood by the community and whether mitigation techniques exist.

The three highest risk systematic errors were studied further and are discussed in subsections below. The PICO team used simulation and analysis tools developed for Planck[133] and *CORE*, adapting them for PICO.

Name	Risk	Effect	
Leakage			
Polarization Angle Calibration	5	E→B	See Sect. 2.6.2.
Bandpass Mismatch	4	T→P, E→B	
Beam mismatch	4	T→P, E→B	See Sect. 2.6.2
Time Response Accuracy and Stability	4	T→P, E→B	
Readout Cross-talk	4	spurious P	
Chromatic beam shape	4	spurious P	
Gain mismatch	3	T→P	
Cross-polarization	3	E→B	
Stability			
Gain Stability	5	T→P, E→B	See Sect. 2.6.3
Pointing jitter	3	T→P, E→B	
Straylight			
Far Sidelobes	5	spurious P	See Sect. 2.6.4.
Other			
Residual correlated cosmic ray hits	3	increased variance	

Table 4: Systematic errors expected in PICO's measurement of CMB polarization.

2.6.2 Absolute polarization angle calibration

CMB polarization can be rotated due to 1. a birefringent primordial Universe, or a Faraday rotation due a primordial magnetic field [139], 2. birefringent foregrounds, or interaction with the Galactic magnetic field, 3. systematic effects in the instrument, and in particular an error on the direction of polarization measured by each detector. While the first two sources create a rotation that may depend on scale, position and/or frequency, the latter depends mainly on the detector.

A rotation α of the direction of polarization mixes the Q and U Stokes parameters via $Q \pm iU \rightarrow e^{\mp i2\alpha} (Q \pm iU)$ and thus mixes the power spectra and their correlations as illustrated in Fig. 13.

The most recent constraints on cosmological birefringence (**author?**) [141] were limited by uncertainties on the detector orientations. In Planck, the detectors were characterized pre-launch to $\pm 0.9^\circ$ (rel.) $\pm 0.3^\circ$ (abs.) [142]. For PICO, the relative rotation of the detectors will be measured to a few $0.1'$ using the CMB, but the overall rotation is unlikely to be known pre-launch to better than Planck. Known polarized sources, such as the Crab Nebula, are not characterized well enough independently to serve as calibrators; (**author?**) [134] show that the current uncertainty of $0.33^\circ = 20'$ on the Crab polarization orientation, limits a B mode measurement to $r \sim 0.01$, far from PICO's target.

In the absence of other systematics and foregrounds, a polarization rotation error α of $10'$ degrades the error bar of r by 30%, while EB , TB and BB spectra can measure a rotation α at 3σ when $\alpha \sim 0.07, 0.2$ and $0.9'$ respectively on perfectly delensed maps, and $0.25, 0.9$ and $4.5'$ on raw maps.

In principle, the technique of using the TB and EB spectra can detect and measure a global

Name	Risk	Effect	State-of-the-art	Additional Mitigation Needed
Leakage				
Polarization Angle Calibration.....	5	E→B	Knowledge of astrophysical calibrators to 0.3° [134]; ground measurement to 0.9° reconstruction to 0.2° using TB and EB demonstrated by <i>Planck</i> [?].	See Sect. 2.6.2.
Bandpass Mismatch.....	4	T→P, E→B	Precise bandpass measurement[?]; SRoll algorithm[?]; filtering technique[?].	SOA meets req't
Beam mismatch	4	T→P, E→B	See Sect. 2.6.2	none
Time Response Accuracy and Stability.....	4	T→P, E→B	On-orbit reconstruction to 0.1% across a wide signal band[135], residuals corrected as part of beam and map-making algorithm[?].	SOA meets req't
Readout Cross-talk.....	4	spurious P	<i>Planck</i> high-impedance bolometers: 10^{-3} crosstalk did not impact CMB polarization[?]. Cross-talk of low-impedance bolometers is 0.3%[136].	SOA meets req't
Chromatic beam shape	4	spurious P	<i>Planck</i> simulations and parameterization as part of the likelihood.	Mission-specific simulations needed.
Gain mismatch	3	T→P	mission-average relative calibration demonstrated to 10^{-4} to 10^{-5} level [?]	SOA meets req't
Cross-polarization	3	E→B	Degenerate with polarization gain calibration.	SOA meets req't
Stability				
Gain Stability	5	T→P, E→B	Reconstruction of time variability of gain to 0.2% in <i>Planck</i> [?].	See Sect. 2.6.3
Pointing jitter.....	3	T→P, E→B	Pointing reconstruction in <i>Planck</i> to 0.8 and 1.9 arcsec in-scan and cross-scan [137]	SOA meets req't
Straylight				
Far Sidelobes.....	5	spurious P	<i>Planck</i> validated straylight model in anechoic chamber to -80 dB _i [138].	See Sect. 2.6.4.
Other				
Residual correlated cosmic ray hits	3	increased variance	<i>Planck</i> /HFI's 5% percent noise correlation did not impact results[?].	SOA detector design to reduce cosmic ray cross-section; SOA analysis techniques meet req't

Table 5: Systematic errors expected in PICO’s measurement of CMB polarization.

polarization rotation error at levels ($0.1'$) below those affecting r measurements in BB ($> 1'$). However, a future mission should simulate additional aspects, such as delensing, the interaction with foregrounds, and $1/f$ noise in simulating and assessing the impact of an angle calibration error.

2.6.3 Gain Stability

Photometric calibration is the process of converting the raw output of the receivers into astrophysical units via the characterization of the *gain factor* $G(t)$ which we allow to vary with time. In space, the characterization of $G(t)$ uses the dipole. For the PICO concept study, we evaluated the impact of noise in the estimation of $G(t)$ using the tools developed for the Planck/LFI instrument and the CORE mission proposal. The quality of the estimate depends on the noise level of the receivers, but also on the details of the scanning strategy. To analyze the impact of calibration uncertainties on PICO, we performed the following analysis:1. We simulated the observation of the sky, assuming four receivers, the nominal scanning strategy, and $1/f$ noise. The simulated sky contained CMB anisotropies, plus the CMB dipole. 2. We ran the calibration code to fit the dipole against the raw data simulated during step 1. 3. We again simulated the observation of the sky, this time using the values of G computed during step 2, which contain errors due to the presence

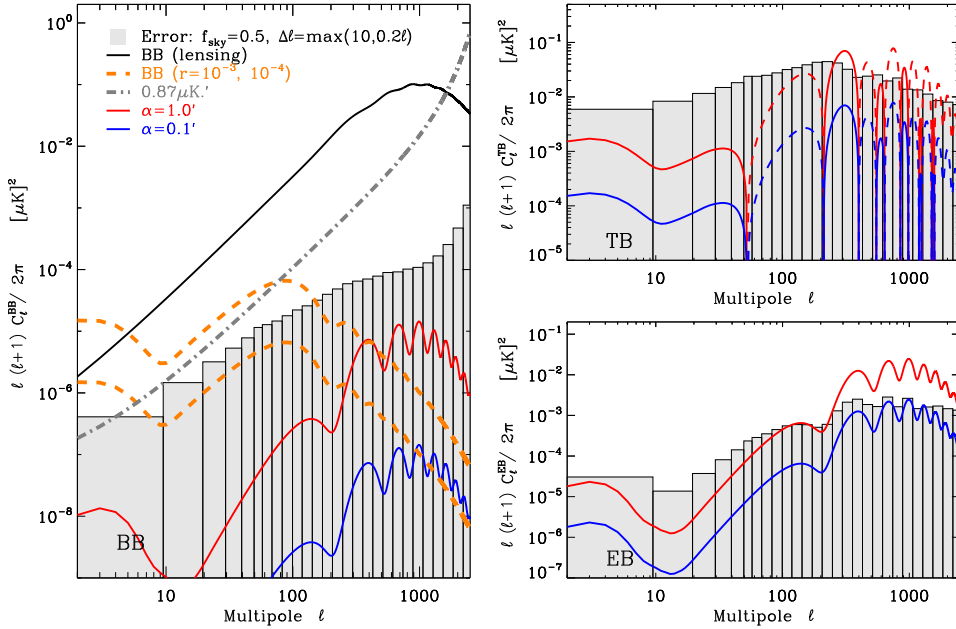


Figure 13: Effect of a rotation of the angle of polarization, assuming the Planck 2018 Λ -CDM best fit model [140] with $\tau = 0.054$ and expected PICO noise performance, assuming perfect delensing.

of noise and the CMB signal.

The presence of large-scale Galactic emission features can bias the estimation of calibration factors. Ideally, a full data analysis pipeline would pair the calibration step with the component separation step, following a schema similar to Planck/LFI’s legacy data processing[143]: the calibration code is followed by a component separation analysis, and these two steps are iterated until the solution converges.

Results of the simulation (neglecting foregrounds) are shown as power spectrum residuals in Fig. 14. We estimate the gain fluctuations to better than 10^{-4} solving for the gain every 40 hours (4 precession periods). The scanning strategy employed by PICO allows for a much better calibration than Planck, thanks to the much faster precession.

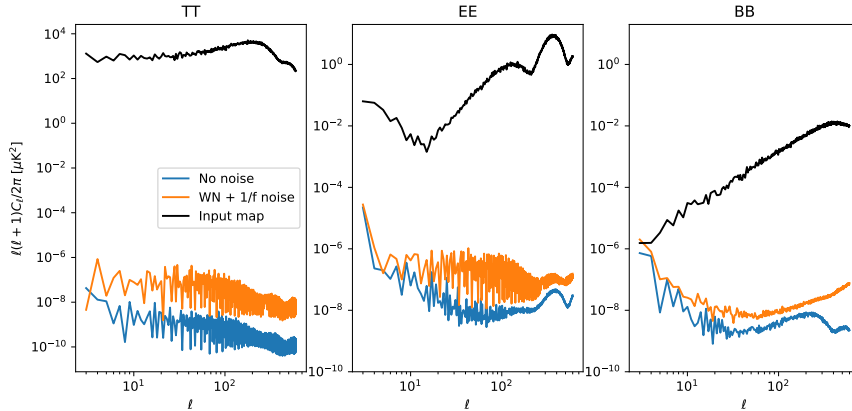


Figure 14: Residual power due to calibration.

2.6.4 Far Sidelobe Pickup

Measurement of each detector's response to signals off axis, which tends to be weak (-80dB less than the peak response) but spread over a very large solid angle, is difficult to do pre-launch, and may not even be done accurately after launch. Nonetheless, this far sidelobe can couple bright Galactic signal from many tens of degrees off-axis and confuse it with polarized signal from the CMB off the Galactic plane.

To evaluate this systematic error, GRASP software⁴ was used to compute the PICO telescope's response over the full sky. This full-sky beam was convolved with a polarized Galactic signal and a full PICO mission scan using the simulation pipeline. The far sidelobe pickup was estimated to contribute less than XXX to the B-mode angular power spectrum and thus an error in r of YYY.

Due to the difficulties of measuring this beam, physical optics simulation capabilities must be maintained and validated as well as possible with on-orbit data.

2.6.5 Key Findings

Properly modeling, engineering for, and controlling the effects of systematic errors in a next-generation CMB probe is critical. As of today, we conclude that there is a clear path to demonstrate that state-of-the-art technology and data processing can take advantage of the L2 environment and control systematic errors to a level that enables the science goals of PICO. In particular we note:

- The raw sensitivity of the instrument should include enough margin that data subsets can independently achieve the science goals. This allows testing of the results in the data analysis and additional data cuts, if needed.
- NASA's support of ground-based and suborbital CMB missions will mitigate risk to a future space mission as PICO by continuing to develop analysis techniques and technology for mitigation of systematic errors.
- In a PICO mission's phase A, a complete end-to-end system-level simulation software facility would be developed to assist the team in setting requirements and conducting trades between subsystem requirements while realistically accounting for post-processing mitigation. Any future CMB mission is likely to have similar orbit and scan characteristics to those of PICO, thus there is an opportunity for NASA and the CMB community to invest in further development of this capability now.

2.7 Measurement Requirements (2 pgs, Hanany & Trangsrud)

The set of physical parameters and observables that derive from the PICO science objectives place requirements on the depth of the mission, the fraction of sky the instrument scans, the frequency range the instrument probes and the number of frequency bands, the angular resolution provided by the reflectors, and the specific pattern with which PICO will observe the sky. We discuss each of these aspects.

• **Depth** We quantify survey depth in terms of the RMS fluctuations that would give a signal-to-noise ratio of 1 on a sky pixel that is 1 arcminute on a side. Depth in any frequency band is determined by detector sensitivity, the number of detectors in the focal plane, the sky area covered, and the duration of the mission. The science objective driving the depth requirement is SO1,

⁴<https://www.ticra.com>

the search for the IGW signal which requires a depth of $0.87 \mu\text{K} \cdot \text{arcmin}$. This requirement is a combination of the low-level of the signal, the need to separate the various signals detected in each band, and the need to detect and subtract systematic effects to the required levels.

- **Sky Coverage** There are several science goals driving a full sky survey for PICO. The term 'full sky' refers to the entire area of sky available after separating other astrophysical sources of confusion. In practice this implies an area of 50-70% of the full sky for probing non-Galactic signals, and the rest of the sky for achieving the Galactic science goals.

(1) Probing the optical depth to the epoch of reionization (STM SO5) requires full sky coverage as the signal peaks in the EE power spectrum on angular scales of 20 to 90 degrees. Measuring this optical depth to limits imposed by the statics of the small number of available ℓ modes is crucial for minimizing the error on the neutrino mass measurement.

(2) If $r \neq 0$, the BB power spectrum due to IGW (STM SO1) also has a local maximum in the same range of angular scales (20 to 90 degrees). For $r \gtrsim 0.001$ (CHECK) this local maximum is at a higher level than the BB lensing spectrum, making this range of scales appealing to survey, as there is no need to separate the signatures of two cosmological signals.

(3) The PICO constraint on N_{eff} (STM SO4) requires a determination of the EE power spectrum to limits imposed by the statics of available ℓ modes. Full sky coverage is required to achieve this limit. (4) PICO's survey of the Galactic plane and regions outside of it is essential to achieving its Galactic structure and star formation science goals (SO6, 7, 8).

- **Frequency Bands** The multitude of astrophysical signals that PICO will characterize determine the frequency range and number of sub-bands that PICO uses. The IGW signal peaks in the frequency range between 30 and 300 GHz. However, Galactic signals, which are themselves signals PICO strives to characterize, are a source of confusion for the IGW. The Galactic signals and the IGW are separable using their spectral signature. Simulations indicate that 21 bands, each with $\sim 25\%$ bandwidth, that are spread across the range of 20 - 800 GHz can achieve the separation at the level of fidelity required by PICO.

Characterizing the Galactic signals, specifically the make up of Galactic dust (SO7), requires spectral characterization of galactic dust in frequencies between 100 and 800 GHz. [Aren't there synchrotron questions that are answerable with spectral information?](#)

- **Resolution** Several science objectives require an aperture of 1.5 m and the resolution listed in Table 1. To reach $\sigma(r) = ??$ we will need to 'delens' the E- and B-mode maps that PICO will generate; see Section ???. Delensing is enabled with a map that has a native resolution of 2-3 arcminutes at frequencies between 100 and 300 GHz. Similar resolution is required to achieve the constraints on the number of light relics (SO??), which will be extracted from the EE power spectrum at multipoles $100 \lesssim \ell \lesssim 2500$. The process of delensing may be affected by other signals, primarily the signal due to Galactic dust. It is thus required to map Galactic dust to at least the same resolution as at 300 GHz. Higher resolution is mandated by science objectives 6,7, and 8, which require resolution of 1 arcminute at 800 GHz. We have thus chosen to implement diffracted limited resolution between 20 and 800 GHz.

- **Sky Scan Pattern** [polarization systematics, 1/f noise](#)

3 Instrument (6 pgs, Hanany & Trangsrud)

Telescope (Hanany / Young), focal plane (Hanany / Young), cooling (Trangsrud), readout (O'Brient)
Review: Bock, Hubmayr, Suzuki,

4 Mission (5 pgs, Trangsrud)

To be included: mission architecture, spacecraft and subsystems, orbit, attitude control and determination (Trangsrud)

5 Technology Maturation (4 pgs, O'Brient & Trangsrud)

Requirements, planned activities, schedules and milestones, estimated cost (O'Brient?)

For each technology include:

- Requirements
- Planned activities
- Schedule and Milestones
- Estimated Cost

6 Management, Risk, Heritage, and Cost (4 pgs, Trangsrud)

cost, risk, heritage (Trangsrud)

References

- [1] G. Steigman. Cosmology confronts particle physics. *Annual Review of Nuclear and Particle Science*, 29:313–338, 1979.
- [2] M. Bolz, A. Brandenburg, and W. Buchmuller. Thermal production of gravitinos. *Nucl. Phys.*, B606:518–544, 2001. [Erratum: Nucl. Phys.B790,336(2008)].
- [3] Christopher Brust, David E. Kaplan, and Matthew T. Walters. New Light Species and the CMB. *JHEP*, 12:058, 2013.
- [4] Daniel Baumann, Daniel Green, and Benjamin Wallisch. A New Target for Cosmic Axion Searches. *Phys. Rev. Lett.*, 117(17):171301, 2016.
- [5] Daniel Green, Joel Meyers, and Alexander van Engelen. CMB Delensing Beyond the B Modes. *ArXiv e-prints*, 2016.
- [6] Cora Dvorkin, Kfir Blum, and Marc Kamionkowski. Constraining Dark Matter-Baryon Scattering with Linear Cosmology. *Phys. Rev.*, D89(2):023519, 2014.
- [7] Francis-Yan Cyr-Racine, Roland de Putter, Alvise Raccanelli, and Kris Sigurdson. Constraints on Large-Scale Dark Acoustic Oscillations from Cosmology. *Phys. Rev.*, D89(6):063517, 2014.
- [8] Manuel A. Buen-Abad, Gustavo Marques-Tavares, and Martin Schmaltz. Non-Abelian dark matter and dark radiation. *Phys. Rev.*, D92(2):023531, 2015.
- [9] Julien Lesgourgues, Gustavo Marques-Tavares, and Martin Schmaltz. Evidence for dark matter interactions in cosmological precision data? *JCAP*, 1602(02):037, 2016.
- [10] Planck Collaboration, N. Aghanim, M. Ashdown, J. Aumont, C. Baccigalupi, M. Ballardini, A. J. Banday, R. B. Barreiro, N. Bartolo, S. Basak, R. Battye, K. Benabed, J.-P. Bernard, M. Bersanelli, P. Bielewicz, J. J. Bock, A. Bonaldi, L. Bonavera, J. R. Bond, J. Borrill, F. R. Bouchet, F. Boulanger, M. Bucher, C. Burigana, R. C. Butler, E. Calabrese, J.-F. Cardoso, J. Carron, A. Challinor, H. C. Chiang, L. P. L. Colombo, C. Combet, B. Comis, A. Coulais, B. P. Crill, A. Curto, F. Cuttaia, R. J. Davis, P. de Bernardis, A. de Rosa, G. de Zotti, J. Delabrouille, J.-M. Delouis, E. Di Valentino, C. Dickinson, J. M. Diego, O. Doré, M. Doussis, A. Ducout, X. Dupac, G. Efstathiou, F. Elsner, T. A. Enßlin, H. K. Eriksen, E. Falgarone, Y. Fantaye, F. Finelli, F. Forastieri, M. Frailis, A. A. Fraisse, E. Franceschi, A. Frolov, S. Galeotta, S. Galli, K. Ganga, R. T. Génova-Santos, M. Gerbino, T. Ghosh, J. González-Nuevo, K. M. Górski, S. Gratton, A. Gruppuso, J. E. Gudmundsson, F. K. Hansen, G. Helou, S. Henrot-Versillé, D. Herranz, E. Hivon, Z. Huang, S. Ilic, A. H. Jaffe, W. C. Jones, E. Keihänen, R. Keskitalo, T. S. Kisner, L. Knox, N. Krachmalnicoff, M. Kunz, H. Kurki-Suonio, G. Lagache, J.-M. Lamarre, M. Langer, A. Lasenby, M. Lattanzi, C. R. Lawrence, M. Le Jeune, J. P. Leahy, F. Levrier, M. Liguori, P. B. Lilje, M. López-Caniego, Y.-Z. Ma, J. F. Macías-Pérez, G. Maggio, A. Mangilli, M. Maris, P. G. Martin, E. Martínez-González, S. Matarrese, N. Mauri, J. D. McEwen, P. R. Meinhold, A. Melchiorri, A. Mennella,

- M. Migliaccio, M.-A. Miville-Deschénes, D. Molinari, A. Moneti, L. Montier, G. Morganante, A. Moss, S. Mottet, P. Naselsky, P. Natoli, C. A. Oxborrow, L. Pagano, D. Paoletti, B. Partridge, G. Patanchon, L. Patrizii, O. Perdereau, L. Perotto, V. Pettorino, F. Piacentini, S. Plaszczynski, L. Polastri, G. Polenta, J.-L. Puget, J. P. Rachen, B. Racine, M. Reinecke, M. Remazeilles, A. Renzi, G. Rocha, M. Rossetti, G. Roudier, J. A. Rubiño-Martín, B. Ruiz-Granados, L. Salvati, M. Sandri, M. Savelainen, D. Scott, G. Sirri, R. Sunyaev, A.-S. Suur-Uski, J. A. Tauber, M. Tenti, L. Toffolatti, M. Tomasi, M. Tristram, T. Trombetti, J. Valiviita, F. Van Tent, L. Vibert, P. Vielva, F. Villa, N. Vittorio, B. D. Wandelt, R. Watson, I. K. Wehus, M. White, A. Zacchei, and A. Zonca. Planck intermediate results. XLVI. Reduction of large-scale systematic effects in HFI polarization maps and estimation of the reionization optical depth. *ArXiv e-prints*, May 2016.
- [11] Manoj Kaplinghat, Lloyd Knox, and Yong-Seon Song. Determining neutrino mass from the CMB alone. *Phys. Rev. Lett.*, 91:241301, 2003.
 - [12] Michael Levi et al. The DESI Experiment, a whitepaper for Snowmass 2013. *ArXiv e-prints*, 2013.
 - [13] Lawrence M. Widrow. Origin of galactic and extragalactic magnetic fields. *Rev. Mod. Phys.*, 74:775–823, 2002.
 - [14] Lawrence M. Widrow, Dongsu Ryu, Dominik R. G. Schleicher, Kandaswamy Subramanian, Christos G. Tsagas, and Rudolf A. Treumann. The First Magnetic Fields. *Space Sci. Rev.*, 166:37–70, 2012.
 - [15] Dario Grasso and Hector R. Rubinstein. Magnetic fields in the early universe. *Phys. Rept.*, 348:163–266, 2001.
 - [16] T. Vachaspati. Magnetic fields from cosmological phase transitions. *Phys. Lett.*, B265:258–261, 1991.
 - [17] Michael S. Turner and Lawrence M. Widrow. Inflation Produced, Large Scale Magnetic Fields. *Phys. Rev.*, D37:2743, 1988.
 - [18] Bharat Ratra. Cosmological ‘seed’ magnetic field from inflation. *Astrophys. J.*, 391:L1–L4, 1992.
 - [19] Andres Diaz-Gil, Juan Garcia-Bellido, Margarita Garcia Perez, and Antonio Gonzalez-Arroyo. Magnetic field production during preheating at the electroweak scale. *Phys. Rev. Lett.*, 100:241301, 2008.
 - [20] Neil Barnaby, Ryo Namba, and Marco Peloso. Observable non-gaussianity from gauge field production in slow roll inflation, and a challenging connection with magnetogenesis. *Phys. Rev.*, D85:123523, 2012.
 - [21] Andrew J. Long, Eray Sabancilar, and Tanmay Vachaspati. Leptogenesis and Primordial Magnetic Fields. *JCAP*, 1402:036, 2014.

- [22] Ruth Durrer and Andrii Neronov. Cosmological Magnetic Fields: Their Generation, Evolution and Observation. *Astron. Astrophys. Rev.*, 21:62, 2013.
- [23] Arthur Kosowsky and Abraham Loeb. Faraday rotation of microwave background polarization by a primordial magnetic field. *Astrophys.J.*, 469:1–6, 1996.
- [24] Antony Lewis. CMB anisotropies from primordial inhomogeneous magnetic fields. *Phys. Rev.*, D70:043011, 2004.
- [25] Alex Zucca, Yun Li, and Levon Pogosian. Constraints on Primordial Magnetic Fields from Planck combined with the South Pole Telescope CMB B-mode polarization measurements. *ArXiv e-prints*, 2016.
- [26] N. Oppermann et al. An improved map of the Galactic Faraday sky. *Astron. Astrophys.*, 542:A93, 2012.
- [27] Soma De, Levon Pogosian, and Tanmay Vachaspati. CMB Faraday rotation as seen through the Milky Way. *Phys. Rev.*, D88(6):063527, 2013.
- [28] Levon Pogosian. Searching for primordial magnetism with multifrequency cosmic microwave background experiments. *Mon. Not. Roy. Astron. Soc.*, 438(3):2508–2512, 2014.
- [29] S. M. Carroll. Quintessence and the Rest of the World: Suppressing Long-Range Interactions. *Physical Review Letters*, 81:3067–3070, October 1998.
- [30] Marc Kamionkowski. How to De-Rotate the Cosmic Microwave Background Polarization. *Phys. Rev. Lett.*, 102:111302, 2009.
- [31] Vera Gluscevic, Marc Kamionkowski, and Asantha Cooray. De-Rotation of the Cosmic Microwave Background Polarization: Full-Sky Formalism. *Phys. Rev.*, D80:023510, 2009.
- [32]
- [33] A. P. S. Yadav, R. Biswas, M. Su, and M. Zaldarriaga. Constraining a spatially dependent rotation of the cosmic microwave background polarization. *Phys. Rev. D.*, 79(12):123009–+, June 2009.
- [34] Peter A. R. Ade et al. POLARBEAR Constraints on Cosmic Birefringence and Primordial Magnetic Fields. *Phys. Rev.*, D92:123509, 2015.
- [35] Planck Collaboration, N. Aghanim, Y. Akrami, M. Ashdown, J. Aumont, C. Baccigalupi, M. Ballardini, A. J. Banday, R. B. Barreiro, N. Bartolo, S. Basak, K. Benabed, J.-P. Bernard, M. Bersanelli, P. Bielewicz, J. J. Bock, J. R. Bond, J. Borrill, F. R. Bouchet, F. Boulanger, M. Bucher, C. Burigana, E. Calabrese, J.-F. Cardoso, J. Carron, A. Challinor, H. C. Chiang, L. P. L. Colombo, C. Combet, B. P. Crill, F. Cuttaia, P. de Bernardis, G. de Zotti, J. Delabrouille, E. Di Valentino, J. M. Diego, O. Doré, M. Douspis, A. Ducout, X. Dupac, G. Efstathiou, F. Elsner, T. A. Enßlin, H. K. Eriksen, Y. Fantaye, R. Fernandez-Cobos, F. Forastieri, M. Frailis, A. A. Fraisse, E. Franceschi, A. Frolov, S. Galeotta, S. Galli, K. Ganga, R. T. Génova-Santos, M. Gerbino, T. Ghosh, J. González-Nuevo, K. M. Górski,

- S. Gratton, A. Gruppuso, J. E. Gudmundsson, J. Hamann, W. Handley, F. K. Hansen, D. Herranz, E. Hivon, Z. Huang, A. H. Jaffe, W. C. Jones, A. Karakci, E. Keihänen, R. Keskitalo, K. Kiiveri, J. Kim, L. Knox, N. Krachmalnicoff, M. Kunz, H. Kurki-Suonio, G. Lagache, J.-M. Lamarre, A. Lasenby, M. Lattanzi, C. R. Lawrence, M. Le Jeune, F. Levrier, A. Lewis, M. Liguori, P. B. Lilje, V. Lindholm, M. López-Caniego, P. M. Lubin, Y.-Z. Ma, J. F. Macías-Pérez, G. Maggio, D. Maino, N. Mandolesi, A. Mangilli, A. Marcos-Caballero, M. Maris, P. G. Martin, E. Martínez-González, S. Matarrese, N. Mauri, J. D. McEwen, A. Melchiorri, A. Mennella, M. Migliaccio, M.-A. Miville-Deschénes, D. Molinari, A. Moneti, L. Montier, G. Morgante, A. Moss, P. Natoli, L. Pagano, D. Paoletti, B. Partridge, G. Patanchon, F. Perrotta, V. Pettorino, F. Piacentini, L. Polastri, G. Polenta, J.-L. Puget, J. P. Rachén, M. Reinecke, M. Remazeilles, A. Renzi, G. Rocha, C. Rosset, G. Roudier, J. A. Rubiño-Martín, B. Ruiz-Granados, L. Salvati, M. Sandri, M. Savelainen, D. Scott, C. Sirignano, R. Sunyaev, A.-S. Suur-Uiski, J. A. Tauber, D. Tavagnacco, M. Tenti, L. Toffolatti, M. Tomasi, T. Trombetti, J. Valiviita, B. Van Tent, P. Vielva, F. Villa, N. Vittorio, B. D. Wandelt, I. K. Wehus, M. White, S. D. M. White, A. Zacchei, and A. Zonca. Planck 2018 results. VIII. Gravitational lensing. *ArXiv e-prints*, July 2018.
- [36] U. Seljak and C. M. Hirata. Gravitational lensing as a contaminant of the gravity wave signal in the CMB. *Phys. Rev. D.*, 69(4):043005, February 2004.
- [37] K. M. Smith, D. Hanson, M. LoVerde, C. M. Hirata, and O. Zahn. Delensing CMB polarization with external datasets. *JCAP*, 6:014, June 2012.
- [38] E. J. Baxter, R. Keisler, S. Dodelson, K. A. Aird, S. W. Allen, M. L. N. Ashby, M. Bautz, M. Bayliss, B. A. Benson, L. E. Bleem, S. Bocquet, M. Brodwin, J. E. Carlstrom, C. L. Chang, I. Chiu, H.-M. Cho, A. Clocchiatti, T. M. Crawford, A. T. Crites, S. Desai, J. P. Dietrich, T. de Haan, M. A. Dobbs, R. J. Foley, W. R. Forman, E. M. George, M. D. Gladders, A. H. Gonzalez, N. W. Halverson, N. L. Harrington, C. Hennig, H. Hoekstra, G. P. Holder, W. L. Holzapfel, Z. Hou, J. D. Hrubes, C. Jones, L. Knox, A. T. Lee, E. M. Leitch, J. Liu, M. Lueker, D. Luong-Van, A. Mantz, D. P. Marrone, M. McDonald, J. J. McMahon, S. S. Meyer, M. Millea, L. M. Mocanu, S. S. Murray, S. Padin, C. Pryke, C. L. Reichardt, A. Rest, J. E. Ruhl, B. R. Saliwanchik, A. Saro, J. T. Sayre, K. K. Schaffer, E. Shirokoff, J. Song, H. G. Spieler, B. Stalder, S. A. Stanford, Z. Staniszewski, A. A. Stark, K. T. Story, A. van Engelen, K. Vanderlinde, J. D. Vieira, A. Vikhlinin, R. Williamson, O. Zahn, and A. Zenteno. A Measurement of Gravitational Lensing of the Cosmic Microwave Background by Galaxy Clusters Using Data from the South Pole Telescope. *Ap. J.*, 806:247, June 2015.
- [39] M. Madhavacheril, N. Sehgal, R. Allison, N. Battaglia, and hysical Review Letters. 114(15):151302, April 2015.
- [40] Planck Collaboration, P. A. R. Ade, N. Aghanim, M. Arnaud, M. Ashdown, J. Aumont, C. Baccigalupi, A. J. Banday, R. B. Barreiro, J. G. Bartlett, and et al. Planck 2015 results. XXIV. Cosmology from Sunyaev-Zeldovich cluster counts. *Astron. Astrophys.*, 594:A24, September 2016.
- [41] J.-B. Melin and J. G. Bartlett. Measuring cluster masses with CMB lensing: a statistical approach. *Astron. Astrophys.*, 578:A21, June 2015.

- [42] U. Seljak. Extracting Primordial Non-Gaussianity without Cosmic Variance. *Physical Review Letters*, 102(2):021302, January 2009.
- [43] M. Schmittfull and U. Seljak. Parameter constraints from cross-correlation of CMB lensing with galaxy clustering. *Phys. Rev. D.*, 97(12):123540, June 2018.
- [44] M. Alvarez, T. Baldauf, J. R. Bond, N. Dalal, R. de Putter, O. Doré, D. Green, C. Hirata, Z. Huang, D. Huterer, D. Jeong, M. C. Johnson, E. Krause, M. Loverde, J. Meyers, P. D. Meerburg, L. Senatore, S. Shandera, E. Silverstein, A. Slosar, K. Smith, M. Zaldarriaga, V. Assassi, J. Braden, A. Hajian, T. Kobayashi, G. Stein, and A. van Engelen. Testing Inflation with Large Scale Structure: Connecting Hopes with Reality. *ArXiv e-prints*, December 2014.
- [45] A. Brandenburg and K. Subramanian. Astrophysical magnetic fields and nonlinear dynamo theory. *Phys. Rep.*, 417:1–209, October 2005.
- [46] Planck Collaboration, R. Adam, P. A. R. Ade, N. Aghanim, Y. Akrami, M. I. R. Alves, F. Argüeso, M. Arnaud, F. Arroja, M. Ashdown, J. Aumont, C. Baccigalupi, M. Ballardini, A. J. Banday, R. B. Barreiro, J. G. Bartlett, N. Bartolo, S. Basak, P. Battaglia, E. Battaner, R. Battye, K. Benabed, A. Benoît, A. Benoit-Lévy, J. P. Bernard, M. Bersanelli, B. Bertinourt, P. Bielewicz, I. Bikmaev, J. J. Bock, H. Böhringer, A. Bonaldi, L. Bonavera, J. R. Bond, J. Borrill, F. R. Bouchet, F. Boulanger, M. Bucher, R. Burenin, C. Burigana, R. C. Butler, E. Calabrese, J. F. Cardoso, P. Carvalho, B. Casaponsa, G. Castex, A. Catalano, A. Challinor, A. Chamballu, R. R. Chary, H. C. Chiang, J. Chluba, G. Chon, P. R. Christensen, S. Church, M. Clemens, D. L. Clements, S. Colombi, L. P. L. Colombo, C. Combet, B. Comis, D. Contreras, F. Couchot, A. Coulais, B. P. Crill, M. Cruz, A. Curto, F. Cuttaia, L. Danese, R. D. Davies, R. J. Davis, P. de Bernardis, A. de Rosa, G. de Zotti, J. Delabrouille, J. M. Delouis, F. X. Désert, E. Di Valentino, C. Dickinson, J. M. Diego, K. Dolag, H. Dole, S. Donzelli, O. Doré, M. Doussis, A. Ducout, J. Dunkley, X. Dupac, G. Efstathiou, P. R. M. Eisenhardt, F. Elsner, T. A. Enßlin, H. K. Eriksen, E. Falgarone, Y. Fantaye, M. Farhang, S. Feeney, J. Fergusson, R. Fernandez-Cobos, F. Feroz, F. Finelli, E. Florido, O. Forni, M. Frailis, A. A. Fraisse, C. Franceschet, E. Franceschi, A. Frejsel, A. Frolov, S. Galeotta, S. Galli, K. Ganga, C. Gauthier, R. T. Génova-Santos, M. Gerbino, T. Ghosh, M. Giard, Y. Giraud-Héraud, E. Giusarma, E. Gjerløw, J. González-Nuevo, K. M. Górski, K. J. B. Grainge, S. Gratton, A. Gregorio, A. Gruppuso, J. E. Gudmundsson, J. Hamann, W. Handley, F. K. Hansen, D. Hanson, D. L. Harrison, A. Heavens, G. Helou, S. Henrot-Versillé, C. Hernández-Monteagudo, D. Herranz, S. R. Hildebrandt, E. Hivon, M. Hobson, W. A. Holmes, A. Hornstrup, W. Hovest, Z. Huang, K. M. Huffenberger, G. Hurier, S. Ilić, A. H. Jaffe, T. R. Jaffe, T. Jin, W. C. Jones, M. Juvela, A. Karakci, E. Keihänen, R. Keskitalo, I. Khamitov, K. Kiiveri, J. Kim, T. S. Kisner, R. Kneissl, J. Knoche, L. Knox, N. Krachmalnicoff, M. Kunz, H. Kurki-Suonio, F. Lacasa, G. Lagache, A. Lähteenmäki, J. M. Lamarre, M. Langer, A. Lasenby, M. Lattanzi, C. R. Lawrence, M. Le Jeune, J. P. Leahy, E. Lellouch, R. Leonardi, J. León-Tavares, J. Lesgourgues, F. Levrier, A. Lewis, M. Liguori, P. B. Lilje, M. Lilley, M. Linden-Vørnle, V. Lindholm, H. Liu, M. López-Caniego, P. M. Lubin, Y. Z. Ma, J. F. Macías-Pérez, G. Maggio, D. Maino, D. S. Y. Mak, N. Mandlesi, A. Mangilli, A. Marchini, A. Marcos-Caballero, D. Marinucci, M. Maris, D. J. Marshall, P. G. Martin,

M. Martinelli, E. Martínez- González, S. Masi, S. Matarrese, P. Mazzotta, J. D. McEwen, P. McGeehee, S. Mei, P. R. Meinholt, A. Melchiorri, J. B. Melin, L. Mendes, A. Mennella, M. Migliaccio, K. Mikkelsen, M. Millea, S. Mitra, M. A. Miville- Deschénes, D. Molinari, A. Moneti, L. Montier, R. Moreno, G. Morgante, D. Mortlock, A. Moss, S. Mottet, M. Münchmeyer, D. Munshi, J. A. Murphy, A. Narimani, P. Naselsky, A. Nastasi, F. Nati, P. Natoli, M. Negrello, C. B. Netterfield, H. U. Nørgaard-Nielsen, F. Noviello, D. Novikov, I. Novikov, M. Olamaie, N. Oppermann, E. Orlando, C. A. Oxborrow, F. Paci, L. Pagano, F. Pajot, R. Paladini, S. Pandolfi, D. Paoletti, B. Partridge, F. Pasian, G. Patanchon, T. J. Pearson, M. Peel, H. V. Peiris, V. M. Pelkonen, O. Perdereau, L. Perotto, Y. C. Perrott, F. Perrotta, V. Pettorino, F. Piacentini, M. Piat, E. Pierpaoli, D. Pietrobon, S. Plaszczynski, D. Pogosyan, E. Pointecouteau, G. Polenta, L. Popa, G. W. Pratt, G. Prézeau, S. Prunet, J. L. Puget, J. P. Rachen, B. Racine, W. T. Reach, R. Rebolo, M. Reinecke, M. Remazeilles, C. Renault, A. Renzi, I. Ristorcelli, G. Rocha, M. Roman, E. Romelli, C. Rosset, M. Rossetti, A. Rotti, G. Roudier, B. Rouillé d'Orfeuil, M. Rowan-Robinson, J. A. Rubiño-Martín, B. Ruiz-Granados, C. Rumsey, B. Rusholme, N. Said, V. Salvatelli, L. Salvati, M. Sandri, H. S. Sanghera, D. Santos, R. D. E. Saunders, A. Sauvé, M. Savelainen, G. Savini, B. M. Schaefer, M. P. Schammel, D. Scott, M. D. Seiffert, P. Serra, E. P. S. Shellard, T. W. Shimwell, M. Shiraishi, K. Smith, T. Souradeep, L. D. Spencer, M. Spinelli, S. A. Stanford, D. Stern, V. Stolyarov, R. Stompor, A. W. Strong, R. Sudiwala, R. Sunyaev, P. Sutter, D. Sutton, A. S. Suur-Uski, J. F. Sygnet, J. A. Tauber, D. Tavagnacco, L. Terenzi, D. Texier, L. Toffolatti, M. Tomasi, M. Tornikoski, D. Tramonte, M. Tristram, A. Troja, T. Trombetti, M. Tucci, J. Tuovinen, M. Türler, G. Umana, L. Valenziano, J. Valiviita, F. Van Tent, T. Vassallo, L. Vibert, M. Vidal, M. Viel, P. Vielva, F. Villa, L. A. Wade, B. Walter, B. D. Wandelt, R. Watson, I. K. Wehus, N. Welikala, J. Weller, M. White, S. D. M. White, A. Wilkinson, D. Yvon, A. Zacchei, J. P. Zibin, and A. Zonca. Planck 2015 results. I. Overview of products and scientific results. *Astron. Astrophys.*, 594:A1, September 2016.

- [47] L. M. Fissel, P. A. R. Ade, F. E. Angilè, P. Ashton, S. J. Benton, M. J. Devlin, B. Dober, Y. Fukui, N. Galitzki, N. N. Gandilo, J. Klein, A. L. Korotkov, Z.-Y. Li, P. G. Martin, T. G. Matthews, L. Moncelsi, F. Nakamura, C. B. Netterfield, G. Novak, E. Pascale, F. Poidevin, F. P. Santos, G. Savini, D. Scott, J. A. Shariff, J. Diego Soler, N. E. Thomas, C. E. Tucker, G. S. Tucker, and D. Ward-Thompson. Balloon-Borne Submillimeter Polarimetry of the Vela C Molecular Cloud: Systematic Dependence of Polarization Fraction on Column Density and Local Polarization-Angle Dispersion. *Ap. J.*, 824:134, June 2016.
- [48] B. S. Hensley and P. Bull. Mitigating Complex Dust Foregrounds in Future Cosmic Microwave Background Polarization Experiments. *Ap. J.*, 853:127, February 2018.
- [49] C. H. Smith, C. M. Wright, D. K. Aitken, P. F. Roche, and J. H. Hough. Studies in mid-infrared spectropolarimetry - II. An atlas of spectra. *MNRAS*, 312:327–361, February 2000.
- [50] J. E. Chiar, A. J. Adamson, D. C. B. Whittet, A. Chrysostomou, J. H. Hough, T. H. Kerr, R. E. Mason, P. F. Roche, and G. Wright. Spectropolarimetry of the 3.4 μm Feature in the Diffuse ISM toward the Galactic Center Quintuplet Cluster. *Ap. J.*, 651:268–271, November 2006.

- [51] R. E. Mason, G. S. Wright, A. Adamson, and Y. Pendleton. Spectropolarimetry of the 3.4 μm Absorption Feature in NGC 1068. *Ap. J.*, 656:798–804, February 2007.
- [52] Planck Collaboration Int. XXII. Planck intermediate results. XXII. Frequency dependence of thermal emission from Galactic dust in intensity and polarization. *Astron. Astrophys.*, 576:A107, April 2015.
- [53] P. C. Ashton, P. A. R. Ade, F. E. Angilè, S. J. Benton, M. J. Devlin, B. Dober, L. M. Fissel, Y. Fukui, N. Galitzki, N. N. Gandilo, J. Klein, A. L. Korotkov, Z.-Y. Li, P. G. Martin, T. G. Matthews, L. Moncelsi, F. Nakamura, C. B. Netterfield, G. Novak, E. Pascale, F. Poidevin, F. P. Santos, G. Savini, D. Scott, J. A. Shariff, J. D. Soler, N. E. Thomas, C. E. Tucker, G. S. Tucker, and D. Ward-Thompson. First Observation of the Submillimeter Polarization Spectrum in a Translucent Molecular Cloud. *Ap. J.*, 857:10, April 2018.
- [54] Aaron M. Meisner and Douglas P. Finkbeiner. Modeling Thermal Dust Emission with Two Components: Application to the Planck High Frequency Instrument Maps. *Ap. J.*, 798:88, January 2015.
- [55] V. Guillet, L. Fanciullo, L. Verstraete, F. Boulanger, A. P. Jones, M.-A. Miville-Deschénes, N. Ysard, F. Levrier, and M. Alves. Dust models compatible with Planck intensity and polarization data in translucent lines of sight. *Astron. Astrophys.*, 610:A16, February 2018.
- [56] B. T. Draine and B. Hensley. Magnetic Nanoparticles in the Interstellar Medium: Emission Spectrum and Polarization. *Ap. J.*, 765:159, March 2013.
- [57] C. F. McKee and E. C. Ostriker. Theory of Star Formation. *Ann. Rev. Astron. Astrophys.*, 45:565–687, September 2007.
- [58] R. M. Crutcher, B. Wandelt, C. Heiles, E. Falgarone, and T. H. Troland. Magnetic Fields in Interstellar Clouds from Zeeman Observations: Inference of Total Field Strengths by Bayesian Analysis. *Ap. J.*, 725:466–479, December 2010.
- [59] S. E. Clark, J. E. G. Peek, and M. E. Putman. Magnetically Aligned H I Fibers and the Rolling Hough Transform. *Ap. J.*, 789:82, July 2014.
- [60] S. E. Clark, J. C. Hill, J. E. G. Peek, M. E. Putman, and B. L. Babler. Neutral Hydrogen Structures Trace Dust Polarization Angle: Implications for Cosmic Microwave Background Foregrounds. *Physical Review Letters*, 115(24):241302, December 2015.
- [61] P. M. W. Kalberla, J. Kerp, U. Haud, B. Winkel, N. Ben Bekhti, L. Flöer, and D. Lenz. Cold Milky Way HI Gas in Filaments. *Ap. J.*, 821:117, April 2016.
- [62] P. M. W. Kalberla and J. Kerp. Anisotropies in the HI gas distribution toward 3C 196. *Astron. Astrophys.*, 595:A37, October 2016.
- [63] T. P. Ellsworth-Bowers, E. Rosolowsky, J. Glenn, A. Ginsburg, N. J. Evans, II, C. Battersby, Y. L. Shirley, and B. Svoboda. The Bolocam Galactic Plane Survey. XII. Distance Catalog Expansion Using Kinematic Isolation of Dense Molecular Cloud Structures with $^{13}\text{CO}(1-0)$. *Ap. J.*, 799:29, January 2015.

- [64] J. D. Soler, P. Hennebelle, P. G. Martin, M.-A. Miville-Deschénes, C. B. Netterfield, and L. M. Fissel. An Imprint of Molecular Cloud Magnetization in the Morphology of the Dust Polarized Emission. *Ap. J.*, 774:128, September 2013.
- [65] C.-Y. Chen, P. K. King, and Z.-Y. Li. Change of Magnetic Field-gas Alignment at the Gravity-driven Alfvénic Transition in Molecular Clouds: Implications for Dust Polarization Observations. *Ap. J.*, 829:84, October 2016.
- [66] J. D. Soler, P. A. R. Ade, F. E. Angilè, P. Ashton, S. J. Benton, M. J. Devlin, B. Dober, L. M. Fissel, Y. Fukui, N. Galitzki, N. N. Gandilo, P. Hennebelle, J. Klein, Z.-Y. Li, A. L. Korotkov, P. G. Martin, T. G. Matthews, L. Moncelsi, C. B. Netterfield, G. Novak, E. Pascale, F. Poidevin, F. P. Santos, G. Savini, D. Scott, J. A. Shariff, N. E. Thomas, C. E. Tucker, G. S. Tucker, and D. Ward-Thompson. The relation between the column density structures and the magnetic field orientation in the Vela C molecular complex. *Astron. Astrophys.*, 603:A64, July 2017.
- [67] Planck Collaboration Int. XXXV. *Planck* intermediate results. XXXV. Probing the role of the magnetic field in the formation of structure in molecular clouds. *Astron. Astrophys.*, 586:A138, 2016.
- [68] P. K. King, L. M. Fissel, C.-Y. Chen, and Z.-Y. Li. Modelling dust polarization observations of molecular clouds through MHD simulations. *MNRAS*, 474:5122–5142, March 2018.
- [69] D. F. González-Casanova and A. Lazarian. Velocity Gradients as a Tracer for Magnetic Fields. *Ap. J.*, 835:41, January 2017.
- [70] K. H. Yuen and A. Lazarian. Tracing Interstellar Magnetic Field Using Velocity Gradient Technique: Application to Atomic Hydrogen Data. *Ap. J. Lett.*, 837:L24, March 2017.
- [71] A. Lazarian and K. H. Yuen. Tracing Magnetic Fields with Spectroscopic Channel Maps. *Ap. J.*, 853:96, January 2018.
- [72] L. Davis, Jr. and J. L. Greenstein. The Polarization of Starlight by Aligned Dust Grains. *Ap. J.*, 114:206, September 1951.
- [73] S. Chandrasekhar and E. Fermi. Magnetic Fields in Spiral Arms. *Ap. J.*, 118:113, July 1953.
- [74] R. H. Hildebrand, L. Kirby, J. L. Dotson, M. Houde, and J. E. Vaillancourt. Dispersion of Magnetic Fields in Molecular Clouds. I. *Ap. J.*, 696:567–573, May 2009.
- [75] M. Houde, J. E. Vaillancourt, R. H. Hildebrand, S. Chitsazzadeh, and L. Kirby. Dispersion of Magnetic Fields in Molecular Clouds. II. *Ap. J.*, 706:1504–1516, December 2009.
- [76] B. G. Andersson, A. Lazarian, and John E. Vaillancourt. Interstellar Dust Grain Alignment. *Annual Review of Astronomy and Astrophysics*, 53:501–539, August 2015.
- [77] D. Seifried, S. Walch, S. Reissl, and J. C. Ibáñez-Mejía. SILCC-Zoom: Polarisation and depolarisation in molecular clouds. *submitted to Ap. J.*, April 2018.

- [78] M.-A. Miville-Deschénes, N. Murray, and E. J. Lee. Physical Properties of Molecular Clouds for the Entire Milky Way Disk. *Ap. J.*, 834:57, January 2017.
- [79] HI4PI Collaboration. HI4PI: A full-sky H I survey based on EBHIS and GASS. *Astron. Astrophys.*, 594:A116, October 2016.
- [80] J. E. G. Peek, B. L. Babler, Y. Zheng, S. E. Clark, K. A. Douglas, E. J. Korpela, M. E. Putman, S. Stanimirović, S. J. Gibson, and C. Heiles. The GALFA-H I Survey Data Release 2. *Ap. J. Suppl.*, 234:2, January 2018.
- [81] N. M. McClure-Griffiths, S. Stanimirović, C. Murray, D. Li, J. M. Dickey, E. Vazquez-Semadeni, J. E. G. Peek, M. Putman, S. E. Clark, M. A. Miville-Deschenes, J. Bland-Hawthorn, and L. Staveley-Smith. Galactic and Magellanic Evolution with the SKA. In *Advancing Astrophysics with the Square Kilometre Array (AASKA14)*, page 130, April 2015.
- [82] A. Allen, Z.-Y. Li, and F. H. Shu. Collapse of Magnetized Singular Isothermal Toroids. II. Rotation and Magnetic Braking. *Ap. J.*, 599:363–379, December 2003.
- [83] Z.-Y. Li, R. Krasnopolsky, H. Shang, and B. Zhao. On the Role of Pseudodisk Warping and Reconnection in Protostellar Disk Formation in Turbulent Magnetized Cores. *Ap. J.*, 793:130, October 2014.
- [84] S. Xu and A. Lazarian. Magnetohydrodynamic turbulence and turbulent dynamo in a partially ionized plasma. *New Journal of Physics*, October 2018.
- [85] A. Lazarian. Enhancement and Suppression of Heat Transfer by MHD Turbulence. *Ap. J. Lett.*, 645:L25–L28, July 2006.
- [86] A. Lazarian. Damping of Alfvén Waves by Turbulence and Its Consequences: From Cosmic-ray Streaming to Launching Winds. *Ap. J.*, 833:131, December 2016.
- [87] A. Lazarian and E. T. Vishniac. Reconnection in a Weakly Stochastic Field. *Ap. J.*, 517:700–718, June 1999.
- [88] Planck Collaboration XXVI. Planck 2015 results. XXVI. The Second Planck Catalogue of Compact Sources. *Astron. Astrophys.*, 594:A26, September 2016.
- [89] M. Negrello, S. Amber, A. Amvrosiadis, Z.-Y. Cai, A. Lapi, J. Gonzalez-Nuevo, G. De Zotti, C. Furlanetto, S. J. Maddox, M. Allen, T. Bakx, R. S. Bussmann, A. Cooray, G. Covone, L. Danese, H. Dannerbauer, H. Fu, J. Greenslade, M. Gurwell, R. Hopwood, L. V. E. Koopmans, N. Napolitano, H. Nayyeri, A. Omont, C. E. Petrillo, D. A. Riechers, S. Serjeant, C. Tortora, E. Valiante, G. Verdoes Kleijn, G. Vernardos, J. L. Wardlow, M. Baes, A. J. Baker, N. Bourne, D. Clements, S. M. Crawford, S. Dye, L. Dunne, S. Eales, R. J. Ivison, L. Marchetti, M. J. Michałowski, M. W. L. Smith, M. Vaccari, and P. van der Werf. The Herschel-ATLAS: a sample of 500 μm -selected lensed galaxies over 600 deg^2 . *MNRAS*, 465:3558–3580, March 2017.

- [90] F. Combes, M. Rex, T. D. Rawle, E. Egami, F. Boone, I. Smail, J. Richard, R. J. Ivison, M. Gurwell, C. M. Casey, A. Omont, A. Berciano Alba, M. Dessauges-Zavadsky, A. C. Edge, G. G. Fazio, J.-P. Kneib, N. Okabe, R. Pelló, P. G. Pérez-González, D. Schaerer, G. P. Smith, A. M. Swinbank, and P. van der Werf. A bright $z = 5.2$ lensed submillimeter galaxy in the field of Abell 773. *HLSJ091828.6+514223*. *Astron. Astrophys.*, 538:L4, February 2012.
- [91] T. Treu. Strong Lensing by Galaxies. *Ann. Rev. Astr. Ap.*, 48:87–125, September 2010.
- [92] R. Cañameras, N. P. H. Nesvadba, D. Guery, T. McKenzie, S. König, G. Petitpas, H. Dole, B. Frye, I. Flores-Cacho, L. Montier, M. Negrello, A. Beelen, F. Boone, D. Dicken, G. Lagache, E. Le Floc'h, B. Altieri, M. Béthermin, R. Chary, G. de Zotti, M. Giard, R. Kneissl, M. Krips, S. Malhotra, C. Martinache, A. Omont, E. Pointecouteau, J.-L. Puget, D. Scott, G. Soucail, I. Valtchanov, N. Welikala, and L. Yan. Planck’s dusty GEMS: The brightest gravitationally lensed galaxies discovered with the Planck all-sky survey. *Astron. Astrophys.*, 581:A105, September 2015.
- [93] R. Cañameras, N. Nesvadba, R. Kneissl, B. Frye, R. Gavazzi, S. Koenig, E. Le Floc'h, M. Limousin, I. Oteo, and D. Scott. Planck’s dusty GEMS. IV. Star formation and feedback in a maximum starburst at $z = 3$ seen at 60-pc resolution. *Astron. Astrophys.*, 604:A117, August 2017.
- [94] R. Cañameras, N. P. H. Nesvadba, R. Kneissl, M. Limousin, R. Gavazzi, D. Scott, H. Dole, B. Frye, S. Koenig, E. Le Floc'h, and I. Oteo. Planck’s dusty GEMS. III. A massive lensing galaxy with a bottom-heavy stellar initial mass function at $z = 1.5$. *Astron. Astrophys.*, 600:L3, April 2017.
- [95] M. Rowan-Robinson, W. Saunders, A. Lawrence, and K. Leech. The QMW IRAS galaxy catalogue - A highly complete and reliable IRAS 60-micron galaxy catalogue. *MNRAS*, 253:485–495, December 1991.
- [96] Planck Collaboration XVI. Planck early results. XVI. The Planck view of nearby galaxies. *Astron. Astrophys.*, 536:A16, December 2011.
- [97] R. J. Ivison, A. M. Swinbank, I. Smail, A. I. Harris, R. S. Bussmann, A. Cooray, P. Cox, H. Fu, A. Kovács, M. Krips, D. Narayanan, M. Negrello, R. Neri, J. Peñarrubia, J. Richard, D. A. Riechers, K. Rowlands, J. G. Staguhn, T. A. Targett, S. Amber, A. J. Baker, N. Bourne, F. Bertoldi, M. Bremer, J. A. Calanog, D. L. Clements, H. Dannerbauer, A. Dariush, G. De Zotti, L. Dunne, S. A. Eales, D. Farrah, S. Fleuren, A. Franceschini, J. E. Geach, R. D. George, J. C. Helly, R. Hopwood, E. Ibar, M. J. Jarvis, J.-P. Kneib, S. Maddox, A. Omont, D. Scott, S. Serjeant, M. W. L. Smith, M. A. Thompson, E. Valiante, I. Valtchanov, J. Vieira, and P. van der Werf. Herschel-ATLAS: A Binary HyLIRG Pinpointing a Cluster of Starbursting Protoellipticals. *Ap. J.*, 772:137, August 2013.
- [98] T. Wang, D. Elbaz, E. Daddi, A. Finoguenov, D. Liu, C. Schreiber, S. Martín, V. Strazzullo, F. Valentino, R. van der Burg, A. Zanella, L. Ciesla, R. Gobat, A. Le Brun, M. Pannella, M. Sargent, X. Shu, Q. Tan, N. Cappelluti, and Y. Li. Discovery of a Galaxy Cluster with a Violently Starbursting Core at $z = 2.506$. *Ap. J.*, 828:56, September 2016.

- [99] I. Oteo, R. J. Ivison, L. Dunne, A. Manilla-Robles, S. Maddox, A. J. R. Lewis, G. de Zotti, M. Bremer, D. L. Clements, A. Cooray, H. Dannerbauer, S. Eales, J. Greenslade, A. Omont, I. Perez-Fournón, D. Riechers, D. Scott, P. van der Werf, A. Weiss, and Z.-Y. Zhang. An Extreme Protocluster of Luminous Dusty Starbursts in the Early Universe. *Ap. J.*, 856:72, March 2018.
- [100] M. Negrello, J. Gonzalez-Nuevo, G. De Zotti, M. Bonato, Z.-Y. Cai, D. Clements, L. Danese, H. Dole, J. Greenslade, A. Lapi, and L. Montier. On the statistics of protocluster candidates detected in the Planck all-sky survey. *ArXiv e-prints*, May 2017.
- [101] R. A. Overzier. The realm of the galaxy protoclusters. A review. *Astron. Astrophys. Rev.*, 24:14, November 2016.
- [102] Planck Collaboration XXXIX. Planck intermediate results. XXXIX. The Planck list of high-redshift source candidates. *Astron. Astrophys.*, 596:A100, December 2016.
- [103] S. Alberts, A. Pope, M. Brodwin, D. W. Atlee, Y.-T. Lin, A. Dey, P. R. M. Eisenhardt, D. P. Gettings, A. H. Gonzalez, B. T. Jannuzzi, C. L. Mancone, J. Moustakas, G. F. Snyder, S. A. Stanford, D. Stern, B. J. Weiner, and G. R. Zeimann. The evolution of dust-obscured star formation activity in galaxy clusters relative to the field over the last 9 billion years. *MNRAS*, 437:437–457, January 2014.
- [104] G. Ghisellini, L. Foschini, M. Volonteri, G. Ghirlanda, F. Haardt, D. Burlon, and F. Tavecchio. The blazar S5 0014+813: a real or apparent monster? *MNRAS*, 399:L24–L28, October 2009.
- [105] R. W. Romani, D. Sowards-Emmerd, L. Greenhill, and P. Michelson. Q0906+6930: The Highest Redshift Blazar. *Ap. J. Lett.*, 610:L9–L11, July 2004.
- [106] G. Ghisellini, G. Tagliaferri, T. Sbarato, and N. Gehrels. SDSS J013127.34-032100.1: a candidate blazar with an 11 billion solar mass black hole at $z = 5.18$. *MNRAS*, 450:L34–L38, June 2015.
- [107] B. D. Metzger, P. K. G. Williams, and E. Berger. Extragalactic Synchrotron Transients in the Era of Wide-field Radio Surveys. I. Detection Rates and Light Curve Characteristics. *Ap. J.*, 806:224, June 2015.
- [108] Ben Thorne, Jo Dunkley, David Alonso, and Sigurd Naess. The Python Sky Model: software for simulating the Galactic microwave sky. 2016.
- [109] Brandon Hensley. *On the nature of interstellar grains*. PhD thesis, Princeton University, 2015.
- [110] A. G. Krtsuk, S. D. Ustyugov, and M. L. Norman. The structure and statistics of interstellar turbulence. *New Journal of Physics*, 19(6):065003, June 2017.
- [111] G. Martínez-Solaeche, A. Karakci, and J. Delabrouille. A 3D model of polarized dust emission in the Milky Way. *MNRAS*, 476:1310–1330, May 2018.

- [112] F. Vansyngel, F. Boulanger, T. Ghosh, B. Wandelt, J. Aumont, A. Bracco, F. Levrier, P. G. Martin, and L. Montier. Statistical simulations of the dust foreground to cosmic microwave background polarization. *Astron. Astrophys.*, 603:A62, July 2017.
- [113] J. Delabrouille, M. Betoule, J.-B. Melin, M.-A. Miville-Deschénes, J. Gonzalez-Nuevo, M. Le Jeune, G. Castex, G. de Zotti, S. Basak, M. Ashdown, J. Aumont, C. Baccigalupi, A. J. Banday, J.-P. Bernard, F. R. Bouchet, D. L. Clements, A. da Silva, C. Dickinson, F. Dodu, K. Dolag, F. Elsner, L. Fauvet, G. Faÿ, G. Giardino, S. Leach, J. Lesgourgues, M. Liguori, J. F. Macías-Pérez, M. Massardi, S. Matarrese, P. Mazzotta, L. Montier, S. Mottet, R. Paladini, B. Partridge, R. Piffaretti, G. Prezeau, S. Prunet, S. Ricciardi, M. Roman, B. Schaefer, and L. Toffolatti. The pre-launch Planck Sky Model: a model of sky emission at submillimetre to centimetre wavelengths. *Astron. Astrophys.*, 553:A96, May 2013.
- [114] A. Lewis, A. Challinor, and A. Lasenby. Efficient Computation of Cosmic Microwave Background Anisotropies in Closed Friedmann-Robertson-Walker Models. *Ap. J.*, 538:473–476, August 2000.
- [115] M.-A. Miville-Deschénes, N. Ysard, A. Lavabre, N. Ponthieu, J. F. Macías-Pérez, J. Aumont, and J. P. Bernard. Separation of anomalous and synchrotron emissions using WMAP polarization data. *Astron. Astrophys.*, 490:1093–1102, November 2008.
- [116] A. Kogut, J. Dunkley, C. L. Bennett, O. Doré, B. Gold, M. Halpern, G. Hinshaw, N. Jarosik, E. Komatsu, M. R. Nolta, N. Odegard, L. Page, D. N. Spergel, G. S. Tucker, J. L. Weiland, E. Wollack, and E. L. Wright. Three-Year Wilkinson Microwave Anisotropy Probe (WMAP) Observations: Foreground Polarization. *Ap. J.*, 665:355–362, August 2007.
- [117] C. Dickinson, Y. Ali-Haïmoud, A. Barr, E. S. Battistelli, A. Bell, L. Bernstein, S. Casassus, K. Cleary, B. T. Draine, R. Génova-Santos, S. E. Harper, B. Hensley, J. Hill-Valler, T. Hoang, F. P. Israel, L. Jew, A. Lazarian, J. P. Leahy, J. Leech, C. H. López-Caraballo, I. McDonald, E. J. Murphy, T. Onaka, R. Paladini, M. W. Peel, Y. Perrott, F. Poidevin, A. C. S. Readhead, J.-A. Rubiño-Martín, A. C. Taylor, C. T. Tibbs, M. Todorović, and M. Vidal. The State-of-Play of Anomalous Microwave Emission (AME) research. *New Ast. Rev.*, 80:1–28, February 2018.
- [118] K. M. Górski, E. Hivon, A. J. Banday, B. D. Wandelt, F. K. Hansen, M. Reinecke, and M. Bartelmann. HEALPix: A Framework for High-Resolution Discretization and Fast Analysis of Data Distributed on the Sphere. *Ap. J.*, 622:759–771, April 2005.
- [119] H. K. Eriksen, J. B. Jewell, C. Dickinson, A. J. Banday, K. M. Górski, and C. R. Lawrence. Joint Bayesian Component Separation and CMB Power Spectrum Estimation. *Ap. J.*, 676:10–32, March 2008.
- [120] Planck Collaboration, R. Adam, P. A. R. Ade, N. Aghanim, M. I. R. Alves, M. Arnaud, M. Ashdown, J. Aumont, C. Baccigalupi, A. J. Banday, and et al. Planck 2015 results. X. Diffuse component separation: Foreground maps. *Astron. Astrophys.*, 594:A10, September 2016.

- [121] Planck Collaboration, Y. Akrami, M. Ashdown, J. Aumont, C. Baccigalupi, M. Ballardini, A. J. Banday, R. B. Barreiro, N. Bartolo, S. Basak, K. Benabed, M. Bersanelli, P. Bielewicz, J. R. Bond, J. Borrill, F. R. Bouchet, F. Boulanger, M. Bucher, C. Burigana, E. Calabrese, J.-F. Cardoso, J. Carron, B. Casaponsa, A. Challinor, L. P. L. Colombo, C. Combet, B. P. Crill, F. Cuttaia, P. de Bernardis, A. de Rosa, G. de Zotti, J. Delabrouille, J.-M. Delouis, E. Di Valentino, C. Dickinson, J. M. Diego, S. Donzelli, O. Doré, A. Ducout, X. Dupac, G. Efstathiou, F. Elsner, T. A. Enßlin, H. K. Eriksen, E. Falgarone, R. Fernandez-Cobos, F. Finelli, F. Forastieri, M. Frailis, A. A. Fraisse, E. Franceschi, A. Frolov, S. Galeotta, S. Galli, K. Ganga, R. T. Génova-Santos, M. Gerbino, T. Ghosh, J. González-Nuevo, K. M. Górski, S. Gratton, A. Gruppuso, J. E. Gudmundsson, W. Handley, F. K. Hansen, G. Helou, D. Herranz, Z. Huang, A. H. Jaffe, A. Karakci, E. Keihänen, R. Keskitalo, K. Kiiveri, J. Kim, T. S. Kisner, N. Krachmalnicoff, M. Kunz, H. Kurki-Suonio, G. Lagache, J.-M. Lamarre, A. Lasenby, M. Lattanzi, C. R. Lawrence, M. Le Jeune, F. Levrier, M. Liguori, P. B. Lilje, V. Lindholm, M. López-Caniego, P. M. Lubin, Y.-Z. Ma, J. F. Macías-Pérez, G. Maggio, D. Maino, N. Mandolesi, A. Mangilli, A. Marcos-Caballero, P. G. Martin, E. Martínez-González, S. Matarrese, N. Mauri, J. D. McEwen, P. R. Meinhold, A. Melchiorri, A. Mennella, M. Migliaccio, M.-A. Miville-Deschénes, D. Molinari, A. Moneti, L. Montier, G. Morgante, P. Natoli, F. Oppizzi, L. Pagano, D. Paoletti, B. Partridge, M. Peel, V. Pettorino, F. Piacentini, G. Polenta, J.-L. Puget, J. P. Rachén, M. Reinecke, M. Remazeilles, A. Renzi, G. Rocha, G. Roudier, J. A. Rubiño-Martín, B. Ruiz-Granados, L. Salvati, M. Sandri, M. Savelainen, D. Scott, D. S. Seljebotn, C. Sirignano, L. D. Spencer, A.-S. Suur-Uski, J. A. Tauber, D. Tavagnacco, M. Tenti, H. Thommesen, L. Toffolatti, M. Tomasi, T. Trombetti, J. Valiviita, B. Van Tent, P. Vielva, F. Villa, N. Vittorio, B. D. Wandelt, I. K. Wehus, A. Zacchei, and A. Zonca. Planck 2018 results. IV. Diffuse component separation. *ArXiv e-prints*, July 2018.
- [122] M. Remazeilles, C. Dickinson, H. K. K. Eriksen, and I. K. Wehus. Sensitivity and foreground modelling for large-scale cosmic microwave background B-mode polarization satellite missions. *MNRAS*, 458:2032–2050, May 2016.
- [123] M. Remazeilles, C. Dickinson, H. K. Eriksen, and I. K. Wehus. Joint Bayesian estimation of tensor and lensing B modes in the power spectrum of CMB polarization data. *MNRAS*, 474:3889–3897, March 2018.
- [124] W. Hu, M. M. Hedman, and M. Zaldarriaga. Benchmark parameters for CMB polarization experiments. *Phys. Rev. D.*, 67:043004–+, February 2003. astro-ph/0210096.
- [125] M. Shimon, B. Keating, N. Ponthieu, and E. Hivon. CMB polarization systematics due to beam asymmetry: Impact on inflationary science. *Phys. Rev. D.*, 77(8):083003–+, April 2008.
- [126] A. P. S. Yadav, M. Su, and M. Zaldarriaga. Primordial B-mode diagnostics and self-calibrating the CMB polarization. *Phys. Rev. D.*, 81(6):063512–+, March 2010.
- [127] Bicep2 Collaboration, P. A. R. Ade, R. W. Aikin, D. Barkats, S. J. Benton, C. A. Bischoff, J. J. Bock, J. A. Brevik, I. Buder, E. Bullock, C. D. Dowell, L. Duband, J. P. Filippini, S. Fliescher, S. R. Golwala, M. Halpern, M. Hasselfield, S. R. Hildebrandt, G. C. Hilton,

- K. D. Irwin, K. S. Karkare, J. P. Kaufman, B. G. Keating, S. A. Kernasovskiy, J. M. Kovac, C. L. Kuo, E. M. Leitch, M. Lueker, C. B. Netterfield, H. T. Nguyen, R. O'Brient, R. W. Ogburn, IV, A. Orlando, C. Pryke, S. Richter, R. Schwarz, C. D. Sheehy, Z. K. Staniszewski, R. V. Sudiwala, G. P. Teply, J. E. Tolan, A. D. Turner, A. G. Vieregg, C. L. Wong, and K. W. Yoon. Bicep2 III: Instrumental Systematics. *Ap. J.*, 814:110, December 2015.
- [128] C. L. Bennett, D. Larson, J. L. Weiland, N. Jarosik, G. Hinshaw, N. Odegard, K. M. Smith, R. S. Hill, B. Gold, M. Halpern, E. Komatsu, M. R. Nolta, L. Page, D. N. Spergel, E. Wollack, J. Dunkley, A. Kogut, M. Limon, S. S. Meyer, G. S. Tucker, and E. L. Wright. Nine-year Wilkinson Microwave Anisotropy Probe (WMAP) Observations: Final Maps and Results. *The Astrophysical Journal Supplement Series*, 208:20, October 2013.
- [129] Planck 2018-I. Planck 2018 results. I. Overview and the Cosmological Legacy of Planck. July 2018.
- [130] M. Hazumi, J. Borrill, Y. Chinone, M. A. Dobbs, H. Fuke, A. Ghribi, M. Hasegawa, K. Hattori, M. Hattori, W. L. Holzapfel, Y. Inoue, K. Ishidoshiro, H. Ishino, K. Karatsu, N. Katayama, I. Kawano, A. Kibayashi, Y. Kibe, N. Kimura, K. Koga, E. Komatsu, A. T. Lee, H. Matsuura, T. Matsumura, S. Mima, K. Mitsuda, H. Morii, S. Murayama, M. Nagai, R. Nagata, S. Nakamura, K. Natsume, H. Nishino, A. Noda, T. Noguchi, I. Ohta, C. Otani, P. L. Richards, S. Sakai, N. Sato, Y. Sato, Y. Sekimoto, A. Shimizu, K. Shinozaki, H. Sugita, A. Suzuki, T. Suzuki, O. Tajima, S. Takada, Y. Takagi, Y. Takei, T. Tomaru, Y. Uzawa, H. Watanabe, N. Yamasaki, M. Yoshida, T. Yoshida, and K. Yotsumoto. LiteBIRD: a small satellite for the study of B-mode polarization and inflation from cosmic background radiation detection. In *Space Telescopes and Instrumentation 2012: Optical, Infrared, and Millimeter Wave*, volume 8442, page 844219, September 2012.
- [131] C. G. R. Wallis, M. L. Brown, R. A. Battye, and J. Delabrouille. Optimal scan strategies for future CMB satellite experiments. *Monthly Notices of the Royal Astronomical Society*, 466(1):425–442, 2017.
- [132] P. Natoli, M. Ashdown, R. Banerji, J. Borrill, A. Buzzelli, G. de Gasperis, J. Delabrouille, E. Hivon, D. Molinari, G. Patanchon, L. Polastri, M. Tomasi, F. R. Bouchet, S. Henrot-Versillé, D. T. Hoang, R. Keskitalo, K. Kiiveri, T. Kisner, V. Lindholm, D. McCarthy, F. Piacentini, O. Perdereau, G. Polenta, M. Tristram, A. Achucarro, P. Ade, R. Allison, C. Baccigalupi, M. Ballardini, A. J. Banday, J. Bartlett, N. Bartolo, S. Basak, D. Baumann, M. Bersanelli, A. Bonaldi, M. Bonato, F. Boulanger, T. Brinckmann, M. Bucher, C. Burigana, Z. Y. Cai, M. Calvo, C. S. Carvalho, M. G. Castellano, A. Challinor, J. Chluba, S. Clesse, I. Colantoni, A. Coppolecchia, M. Crook, G. D'Alessandro, P. de Bernardis, G. De Zotti, E. Di Valentino, J. M. Diego, J. Errard, S. Feeney, R. Fernandez-Cobos, F. Finelli, F. Forastieri, S. Galli, R. Genova-Santos, M. Gerbino, J. González-Nuevo, S. Grandis, J. Greenslade, A. Gruppuso, S. Hagstotz, S. Hanany, W. Handley, C. Hernandez-Monteagudo, C. Hervías-Caimapo, M. Hills, E. Keihänen, T. Kitching, M. Kunz, H. Kurki-Suonio, L. Lamagna, A. Lasenby, M. Lattanzi, J. Lesgourgues, A. Lewis, M. Liguori, M. López-Caniego, G. Luzzi, B. Maffei, N. Mandolesi, E. Martínez-González, C. J. A. P. Martins, S. Masi, S. Matarrese, A. Melchiorri, J. B. Melin, M. Migliaccio, A. Monfardini,

M. Negrello, A. Notari, L. Pagano, A. Paiella, D. Paoletti, M. Piat, G. Pisano, A. Pollo, V. Poulin, M. Quartin, M. Remazeilles, M. Roman, G. Rossi, J. A. Rubino- Martin, L. Salvati, G. Signorelli, A. Tartari, D. Tramonte, N. Trappe, T. Trombetti, C. Tucker, J. Valiviita, R. Van de Weijgaert, B. van Tent, V. Vennin, P. Vielva, N. Vittorio, C. Wallis, K. Young, and M. Zannoni. Exploring cosmic origins with CORE: Mitigation of systematic effects. *Journal of Cosmology and Astro-Particle Physics*, 2018:022, April 2018.

- [133] Planck Collaboration, P. A. R. Ade, N. Aghanim, M. Arnaud, M. Ashdown, J. Aumont, C. Baccigalupi, A. J. Banday, R. B. Barreiro, J. G. Bartlett, and et al. Planck 2015 results. XII. Full focal plane simulations. *Astron. Astrophys.*, 594:A12, September 2016.
- [134] Jonathan Aumont, Juan-Francisco Macias-Perez, Alessia Ritacco, Nicolas Ponthieu, and Anna Mangilli. Absolute calibration of the polarisation angle for future CMB *B*-mode experiments from current and future measurements of the Crab nebula. May 2018.
- [135] P A R Planck Collaboration: Ade, N Aghanim, C Armitage-Caplan, M Arnaud, M Ashdown, F Atrio-Barandela, J Aumont, C Baccigalupi, A J Banday, R B Barreiro, E Battaner, K Benabed, A Benoît, A Benoit-Lévy, J P Bernard, M Bersanelli, P Bielewicz, J Bobin, J J Bock, J R Bond, J Borrill, F R Bouchet, J W Bowyer, M Bridges, M Bucher, C Burigana, J F Cardoso, A Catalano, A Challinor, A Chamballu, R R Chary, L Y Chiang, H C Chiang, P R Christensen, S Church, D L Clements, S Colombi, L P L Colombo, F Couchot, A Coulais, B P Crill, A Curto, F Cuttaia, L Danese, R D Davies, P de Bernardis, A de Rosa, G de Zotti, J Delabrouille, J M Delouis, F X Désert, J M Diego, H Dole, S Donzelli, O Dore, M Douspis, J Dunkley, X Dupac, G Efstathiou, T A Enßlin, H K Eriksen, F Finelli, O Forni, M Frailis, A A Fraisse, E Franceschi, S Galeotta, K Ganga, M Giard, Y Giraud-Héraud, J González-Nuevo, K M Gorski, S Gratton, A Gregorio, A Gruppuso, J E Gudmundsson, J Haissinski, F K Hansen, D Hanson, D Harrison, S Henrot-Versillé, C Hernandez-Monteagudo, D Herranz, S R Hildebrandt, E Hivon, M Hobson, W A Holmes, A Hornstrup, Z Hou, W Hovest, K M Huffenberger, T R Jaffe, A H Jaffe, W C Jones, M Juvela, E Keihänen, R Keskitalo, T S Kisner, R Kneissl, J Knoche, L Knox, M Kunz, H Kurki-Suonio, G Lagache, J M Lamarre, A Lasenby, R J Laureijs, C R Lawrence, R Leonardi, C Leroy, J Lesgourgues, M Liguori, P B Lilje, M Linden-Vørnle, M López-Caniego, P M Lubin, J F Macías-Pérez, C J MacTavish, B Maffei, N Mandolesi, M Maris, D J Marshall, P G Martin, E Martínez-González, S Masi, S Matarrese, T Matsumura, F Matthai, P Mazzotta, P McGehee, A Melchiorri, L Mendes, A Mennella, M Migliaccio, S Mitra, M A Miville-Deschénes, A Moneti, L Montier, G Morgante, D Mortlock, D Munshi, J A Murphy, P Naselsky, F Nati, P Natoli, C B Netterfield, H U Nørgaard-Nielsen, F Noviello, D Novikov, I Novikov, S Osborne, C A Oxborrow, F Paci, L Pagano, F Pajot, D Paoletti, F Pasian, G Patanchon, O Perdereau, L Perotto, F Perrotta, F Piacentini, M Piat, E Pierpaoli, D Pietrobon, S Plaszczynski, E Pointecouteau, A M Polegre, G Polenta, N Ponthieu, L Popa, T Poutanen, G W Pratt, G Prézeau, S Prunet, J L Puget, J P Rachén, M Reinecke, M Remazeilles, C Renault, S Ricciardi, T Riller, I Ristorcelli, G Rocha, C Rosset, G Roudier, M Rowan-Robinson, B Rusholme, M Sandri, D Santos, A Sauvé, G Savini, E P S Sheldar, L D Spencer, J L Starck, V Stolyarov, R Stompor, R Sudiwala, F Sureau, D Sutton, A S Suur-Uski, J F Sygnet, J A Tauber, D Tavagnacco, L Terenzi, M Tomasi, M Tristram, M Tucci, G Umana, L Valenziano, J Valiviita, B Van Tent, P Vielva, F Villa, N Vittorio, L A

Wade, B D Wandelt, D Yvon, A Zacchei, and A Zonca. Planck 2013 results. VII. HFI time response and beams. *arXiv.org*, pages 1–31, March 2013.

- [136] BICEP2 Collaboration, P. A. R. Ade, R. W. Aikin, M. Amiri, D. Barkats, S. J. Benton, C. A. Bischoff, J. J. Bock, J. A. Brevik, I. Buder, E. Bullock, G. Davis, P. K. Day, C. D. Dowell, L. Duband, J. P. Filippini, S. Fliescher, S. R. Golwala, M. Halpern, M. Hasselfield, S. R. Hildebrandt, G. C. Hilton, K. D. Irwin, K. S. Karkare, J. P. Kaufman, B. G. Keating, S. A. Kernasovskiy, J. M. Kovac, C. L. Kuo, E. M. Leitch, N. Llombart, M. Lueker, C. B. Netterfield, H. T. Nguyen, R. O'Brient, IV Ogburn, R. W., A. Orlando, C. Pryke, C. D. Reintsema, S. Richter, R. Schwarz, C. D. Sheehy, Z. K. Staniszewski, K. T. Story, R. V. Sudiwala, G. P. Teply, J. E. Tolan, A. D. Turner, A. G. Vieregg, P. Wilson, C. L. Wong, and K. W. Yoon. BICEP2. II. Experiment and three-year Data Set. *Ap. J.*, 792:62, September 2014.
- [137] Planck Collaboration, N. Aghanim, M. Ashdown, J. Aumont, C. Baccigalupi, M. Ballardini, A. J. Banday, R. B. Barreiro, N. Bartolo, S. Basak, K. Benabed, J.-P. Bernard, M. Bersanelli, P. Bielewicz, A. Bonaldi, L. Bonavera, J. R. Bond, J. Borrill, F. R. Bouchet, F. Boulanger, A. Bracco, C. Burigana, E. Calabrese, J.-F. Cardoso, H. C. Chiang, L. P. L. Colombo, C. Combet, B. Comis, B. P. Crill, A. Curto, F. Cuttaia, R. J. Davis, P. de Bernardis, A. de Rosa, G. de Zotti, J. Delabrouille, J.-M. Delouis, E. Di Valentino, C. Dickinson, J. M. Diego, O. Doré, M. Douspis, A. Ducout, X. Dupac, S. Dusini, G. Efstathiou, F. Elsner, T. A. Enßlin, H. K. Eriksen, E. Falgarone, Y. Fantaye, F. Finelli, M. Frailis, A. A. Fraisse, E. Franceschi, A. Frolov, S. Galeotta, S. Galli, K. Ganga, R. T. Génova-Santos, M. Gerbino, T. Ghosh, M. Giard, J. González-Nuevo, K. M. Górski, A. Gregorio, A. Gruppuso, J. E. Gudmundsson, F. K. Hansen, G. Helou, D. Herranz, E. Hivon, Z. Huang, A. H. Jaffe, W. C. Jones, E. Keihänen, R. Keskitalo, T. S. Kisner, N. Krachmalnicoff, M. Kunz, H. Kurki-Suonio, G. Lagache, A. Lähteenmäki, J.-M. Lamarre, A. Lasenby, M. Lattanzi, C. R. Lawrence, M. Le Jeune, F. Levrier, M. Liguori, P. B. Lilje, M. López-Caniego, P. M. Lubin, J. F. Macías-Pérez, G. Maggio, D. Maino, N. Mandolesi, A. Mangilli, M. Maris, P. G. Martin, E. Martínez-González, S. Matarrese, N. Mauri, J. D. McEwen, A. Melchiorri, A. Mennella, M. Migliaccio, S. Mitra, M.-A. Miville-Deschénes, D. Molinari, A. Moneti, L. Montier, G. Morgante, A. Moss, P. Naselsky, H. U. Nørgaard-Nielsen, C. A. Oxborrow, L. Pagano, D. Paoletti, B. Partridge, L. Patrizii, O. Perdereau, L. Perotto, V. Pettorino, F. Piacentini, S. Plaszczynski, G. Polenta, J.-L. Puget, J. P. Rachen, M. Reinecke, M. Remazeilles, A. Renzi, G. Rocha, M. Rossetti, G. Roudier, J. A. Rubiño-Martín, B. Ruiz-Granados, L. Salvati, M. Sandri, M. Savelainen, D. Scott, C. Sirignano, G. Sirri, L. Stanco, A.-S. Suur-Uski, J. A. Tauber, M. Tenti, L. Toffolatti, M. Tomasi, M. Tristram, T. Trombetti, J. Valiviita, J. Vansyngel, F. Van Tent, P. Vielva, B. D. Wandelt, I. K. Wehus, A. Zacchei, and A. Zonca. Planck intermediate results. L. Evidence for spatial variation of the polarized thermal dust spectral energy distribution and implications for CMB *B*-mode analysis. *ArXiv e-prints*, June 2016.
- [138] J A Tauber, H U Nørgaard-Nielsen, P A R Ade, J Amiri Parian, T Banos, M Bersanelli, C Burigana, A Chamballu, D de Chambure, P R Christensen, O Corre, A Cozzani, B Crill, G Crone, O D'Arcangelo, R Daddato, D Doyle, D Dubruel, G Forma, R Hills, K Huffenberger, A H Jaffe, N Jessen, P Kletzkine, J M Lamarre, J P Leahy, Y Longval, P de Maagt,

- B Maffei, N Mandolesi, J Martí-Canales, A Martín-Polegre, P Martin, L Mendes, J A Murphy, P Nielsen, F Noviello, M Paquay, T Peacocke, N Ponthieu, K Pontoppidan, I Ristorcelli, J B Riti, L Rolo, C Rosset, M Sandri, G Savini, R Sudiwala, M Tristram, L Valenziano, M van der Vorst, K van 't Klooster, F Villa, and V Yurchenko. Planck pre-launch status: The optical system. *Astronomy and Astrophysics*, 520:A2, September 2010.
- [139] Levon Pogosian and Alex Zucca. Searching for primordial magnetic fields with CMB B-modes. *Classical and Quantum Gravity*, 35(12):124004, May 2018.
- [140] Planck 2018-VI. Planck 2018 results. VI. Cosmological parameters. July 2018.
- [141] Planck collaboration. Planck intermediate results. XLIX. Parity-violation constraints from polarization data. *Astronomy and Astrophysics*, 596:A110, December 2016.
- [142] C. Rosset, M. Tristram, N. Ponthieu, P. Ade, J. Aumont, A. Catalano, L. Conversi, F. Couchot, B. P. Crill, F.-X. Désert, K. Ganga, M. Giard, Y. Giraud-Héraud, J. Haïssinski, S. Henrot-Versillé, W. Holmes, W. C. Jones, J.-M. Lamarre, A. Lange, C. Leroy, J. Macías-Pérez, B. Maffei, P. de Marcillac, M.-A. Miville-Deschénes, L. Montier, F. Noviello, F. Pajot, O. Perdereau, F. Piacentini, M. Piat, S. Plaszczynski, E. Pointecouteau, J.-L. Puget, I. Ristorcelli, G. Savini, R. Sudiwala, M. Veneziani, and D. Yvon. Planck pre-launch status: High Frequency Instrument polarization calibration. *A&A*, 520:A13+, September 2010.
- [143] Planck 2018-II. Planck 2018 results. II. Low Frequency Instrument data processing. July 2018.